AI and Labor-Market Reallocation*

Hie Joo Ahn† Nicholas A. Carollo‡

March 26, 2026

Abstract

This paper documents how artificial intelligence shapes the stocks and flows of the U.S. labor market. Combining worker-level AI exposure measures with individual-level CPS micro data and Lightcast job postings, we decompose labor force stocks, worker flows, and market tightness by AI exposure and adoption. AI-exposed workers have lower unemployment rates than non-exposed workers, primarily driven by lower separation rates. Since the introduction of LLMs, AI has increased within-job activity switching while reducing job-to-job transitions among highly exposed workers, suggesting that adjustment occurs primarily through task reorganization within firms alongside a decline in demand for these workers. To quantify AI-driven reallocation pressure, we construct individual-level hirability and separability indices and show that dispersion in job-finding prospects has risen markedly since 2023, owing to AI. AI diffusion is also associated with higher nominal wage growth, whereas AI exposure increases hours worked but AI adoption reduces it in the pre-LLM period. These effects attenuate after the introduction of LLMs, suggesting softer labor demand for highly exposed workers and a reconfiguration of labor input. A Bayesian trend-cycle model of unemployment flows suggests that AI modestly increased the natural rate of unemployment by about a quarter percentage point, albeit with considerable uncertainty.

JEL classification: E24, J21, J62, J64, O33.

Keywords: artificial intelligence, labor market flows, unemployment, mismatch, natural rate of unemployment, reallocation

*The views expressed in this paper are those of the authors and do not necessarily represent the views or policies of the Board of Governors of the Federal Reserve System or its staff.

†Corresponding author. Federal Reserve Board of Governors, 20th Street and Constitution Avenue NW, Washington, DC 20551, U.S.A. Email: econ.hjahn@gmail.com

‡Federal Reserve Board of Governors, 20th Street and Constitution Avenue NW, Washington, DC 20551, U.S.A. Email: carollo.nicholas@gmail.com

We are suffering, not from the rheumatics of old age, but from the growing pains of over-rapid changes, from the painfulness of readjustment between one economic period and another. The increase of technical efficiency has been taking place faster than we can deal with the problem of labour absorption. We are being afflicted with technological unemployment. — Keynes (1930)

1 Introduction

The rapid diffusion of artificial intelligence—and large language models (LLMs) in particular—has prompted significant debate about its consequences for the labor market. Whether AI will predominantly complement human workers, substitute for them, or trigger broad reallocation across occupations and industries remains deeply contested. A growing literature documents the productivity and employment effects of AI for specific worker groups and occupations, but far less is known about how AI reshapes aggregate labor market dynamics and the supply-side of the macro economy: the stocks and flows of employment, unemployment, and nonparticipation, the distribution of hiring and separation probabilities across workers, and by extension, wage inflation and the natural rate of unemployment.

This paper fills this gap by providing the systematic empirical analysis of how AI exposure reshapes the U.S. labor market at the aggregate level. Our approach combines three elements. First, we construct worker-level and job-posting-level measures of AI exposure and adoption. For exposure, we draw on occupation-level scores from Eloundou et al. [2023] and Handa et al. [2025], which characterize the extent to which generative AI can perform the tasks associated with each occupation. For adoption, we compute the share of positions that explicitly require AI-related skills from Lightcast job postings, capturing the extent to which firms have actually integrated AI into production. Second, we assign these measures to individual workers in the Current Population Survey (CPS) using detailed occupation codes, and impute exposure for workers without occupation information—including labor force entrants and young workers without prior work experience, who are precisely the workers most vulnerable to AI-driven displacement yet systematically excluded from occupation-based exposure measures. This approach allows

us to decompose the stocks and flows of labor force status into AI-exposed and AI-nonexposed components while preserving all accounting identities in the aggregate. Third, we combine these individual-level flow rates with occupation-level vacancy data constructed from JOLTS and Lightcast to analyze how AI shapes market tightness across the distribution of AI exposure.

Our analysis produces four main findings. *First*, workers with high AI exposure (high exposure, henceforth) have substantially lower unemployment rates than non-exposed workers—4.0 versus 6.3 percent on average over 2011–2025—primarily driven by lower job separation (EU) rates, despite lower job-finding (UE) rates. In addition, high-exposure workers exhibit higher labor force participation rates and employment-to-population ratios, primarily driven by their lower employment-to-nonparticipation (EN) rates, despite their lower job-finding rates from nonparticipation. The share of workers with high AI exposure is higher in the labor force than in the nonparticipation pool, and also has increased over time. This observation suggests that AI exposure is closely associated with job experiences and job losers with high AI exposure likely remain in active job search.

Second, AI appears to reshape within-firm labor allocation more than it spurs cross-employer reallocation. The rate of activity switches within the job rose disproportionately for the high AI-exposure group, meanwhile worker or job reallocation flows rates of high-exposure workers do not show as noticeable pick up. Indeed, job-to-job transition rates show no increase with AI exposure and have actually declined somewhat for the most highly exposed workers since 2023. This result suggests that AI-driven adjustment is occurring primarily along the intensive margin—through reorganization of tasks within firms—rather than through worker mobility across employers.

Third, the market tightness of high-exposure workers is higher than that of low-exposure workers, but the advantage of AI-exposed workers in terms of market tightness has eroded since 2023. Tightness for high-exposure workers has remained persistently below its pre-COVID level while recovering for low-exposure workers, consistent with weakening labor demand in high-exposure occupations following the introduction of LLMs. These uneven effects of LLMs on labor demand increase dispersion in job-finding rates and labor market outcomes across workers, thereby raising reallocation pressures and the degree of mismatch.

Fourth, to quantify the reallocation pressure associated with AI, we construct individual-

level *hirability* and *separability* indices that capture an individual's estimated probability of transitioning into employment and of losing a job, respectively. The cross-sectional dispersion in the hirability index has risen sharply since 2023, and AI factors account for essentially all of this increase. The dispersion of the separability index, by contrast, shows no comparable increase. Drawing on the theoretical frameworks of Jackman and Roper [1987] and Şahin et al. [2014], we show that increased dispersion in job-finding rates raises structural unemployment even in the absence of changes in the mean job-finding rate, and may signal an increase in the natural rate of unemployment in the post-LLM period.

Fifth, we explore implications for wage growth and hours worked. AI diffusion is associated with higher nominal wage growth, while AI exposure increases hours worked and AI adoption reduces them in the pre-LLM period. These effects attenuate following the introduction of LLMs, suggesting a softening of labor demand for highly exposed workers and a reconfiguration of labor input. In particular, the dampening of wage premia and the reconfiguration of hours worked in high-exposure and high-adoption segments are consistent with a slowdown in hiring for these workers and increased reallocation pressure.

Lastly, we assess AI's effects on the natural rate of unemployment through an unemployment-flows model based on a Bayesian trend–cycle decomposition, an approach in the spirit of previous studies on the natural rate of unemployment, including Tasci [2012], Crump et al. [2019], and Ahn [2023]. After extracting the trend components of unemployment inflows and outflows of workers with high- and low- AI exposure based on the Bayesian model, we feed the trend estimates back into Shimer [2012]' steady-state model of unemployment rate for the two groups of workers to recover the aggregate natural rate of unemployment rate. Reflecting the modest weakening of job finding rate of high-exposure workers relative to that of low-exposure workers, the natural rate is estimated to have risen by a quarter percentage point between 2022:Q4 and 2025:Q4, albeit with considerable uncertainty surrounding this estimate.

This paper distinguishes itself from the existing literature along several dimensions. While most prior work examines AI's effects on specific occupations, firms, or demographic groups [Brynjolfsson et al., 2018, Webb, 2020, Felten et al., 2023, Eloundou et al., 2023, Acemoglu et al., 2022, Hampole et al., 2025, Brynjolfsson et al., 2025a, Hosseini and Lichtinger, 2025, Crane and Soto, 2026], this paper is the first to systematically analyze how AI shapes aggregate U.S. labor

market dynamics through the full stock-flow accounting of employment, unemployment, and nonparticipation. Rather than focusing on employment levels or wages alone, it decomposes all worker transition rates by AI exposure, revealing not just whether AI affects labor market outcomes but how. A key methodological contribution is the imputation of AI exposure for workers without occupation information—including labor force entrants and young workers without prior work experience—who are precisely the workers most vulnerable to AI-driven displacement yet systematically excluded from occupation-based exposure measures. A key empirical finding—that AI-driven reallocation operates primarily through reduced hiring rather than increased separations—speaks to a question prior microeconomic studies only partially address [Brynjolfsson et al., 2025a, Hosseini and Lichtinger, 2025].

The paper also extends the occupation-level adaptive capacity index of Manning and Aguirre [2026] to individual workers, constructing novel hirability and separability indices that track the dispersion in job prospects attributable to AI over time, and uses these to estimate AI's contribution to the natural rate of unemployment via a formal trend-cycle decomposition [Tasci, 2012, Crump et al., 2019, Ahn, 2023]. Finally, the finding that AI increases the switch rate of within-establishment activity but not the job-to-job transition places this paper at the intersection of the micro-AI and macro structural unemployment literature [Lilien, 1982, Abraham and Katz, 1986, Neumann and Topel, 1991], connecting the two through the framework of Jackman and Roper [1987].

Section 2 discusses the theoretical framework that guides our empirical analyses on disparities in labor market outcomes and the reallocation pressure driven by AI. Section 3 describes the datasets used for the empirical analyses. Section 5 reports demographics and labor market outcomes by AI exposure and adoption, focusing on stocks and flows of workers and jobs. Section 7 introduces the individual-level separability and hirability indices and analyzes the extent to which AI contributes to the dispersion in the likelihood of job findings and job separations. Section 8 discusses implications for the natural rate of unemployment and the trend labor force participation rate.

Related literature Our work contributes, first, to a rapidly growing empirical literature on the labor market effects of artificial intelligence. One branch of this literature focuses on identifying

which occupations and industries are potentially exposed to AI-related disruptions based on their task structures [Brynjolfsson et al., 2018, Webb, 2020, Felten et al., 2023, Eloundou et al., 2023]. Recent work in this vein leverages large-scale data on user interactions with LLMs to disentangle which tasks AI may automate and which it may augment [Handa et al., 2025, Tomlinson et al., 2025]. Moving beyond task exposure, [Manning and Aguirre, 2026] develop an occupation-level adaptive capacity index that measures how capable workers are of adjusting to job displacement. The hirability and separability indices we construct in this paper extend this idea to individual workers and allow us to characterize the extent to which AI has already contributed to reallocation pressure in the labor market.

Another branch of literature examines the employment effects of AI exposure for specific occupations and demographic groups. Studies focusing on traditional AI and machine learning applications have generally found small net employment effects and evidence of within-firm task reallocation [Acemoglu et al., 2022, Hampole et al., 2025]. Recent work focusing on the adoption of generative AI, however, has documented adverse employment effects for early-career workers in highly-exposed occupations [Brynjolfsson et al., 2025a, Hosseini and Lichtinger, 2025] and reduced employment growth for coders in particular [Crane and Soto, 2026]. Consistent with our findings, these negative employment effects appear to be the result of reduced hiring rather than increased separations. Our paper complements this microeconomic evidence by providing the first systematic analysis of AI's influence on the aggregate labor market, in particular, its implications for structural unemployment.

In addition to employment effects and reallocation pressure, our analysis also speaks to the effect of AI on structural productivity. Although a number of experimental and quasi-experimental studies have shown that access to LLMs increase the productivity of individual workers across a variety of domains [Brynjolfsson et al., 2025b, Cui et al., 2024, Dell'Acqua et al., 2023, Noy and Zhang, 2023], the implications of task-level gains for aggregate productivity remain highly uncertain. Task-accounting approaches, for example, suggest a wide range of potential contributions to TFP growth ranging from essentially zero [Acemoglu, 2025] to as much as percentage point over the next decade [Filippucci et al., 2025].

Finally, our paper contributes to a broader macro-labor literature on labor market reallocation and the effects of technological change. To begin with the literature on effects of reallocation

on unemployment, Lilien [1982] interprets increases in the dispersion of sectoral employment growth during downturns as evidence of sectoral reallocation, implying that the associated rise in unemployment is largely structural. In contrast, Abraham and Katz [1986] argue that countercyclical dispersion can arise from heterogeneous sensitivities of sectors to aggregate shocks, so that the comovement between employment dispersion and the unemployment rate does not necessarily indicate an increase in structural unemployment during recessions. Different from these views, Neumann and Topel [1991] claim that the low-frequency evolution of sectoral employment shares captures permanent demand shift across industries, creating the persistent reallocation pressure that drives up structural unemployment.[1] By explicitly decomposing the dispersion of employment growth into contributions from the four structural components, we directly isolate the portion that reflects genuine sectoral reallocation pressures relevant for structural unemployment, controlling for cyclical components.

2 Theory on the AI-driven reallocation and mismatch

Section 2.1 presents the Jackman–Roper condition, which links changes in the unemployment rate to dispersion in job-finding probabilities. Section 2.2 extends this framework to allow for heterogeneity in separation rates. Section 2.3 examines the role of AI in shaping the dispersion of unemployment flows. Finally, Section 2.4 discusses the implications for mismatch and structural unemployment.

2.1 Jackman and Roper condition

In their influential study on structural unemployment, Jackman and Roper [1987] demonstrate a link between dispersion in job-finding rates across workers and equilibrium unemployment and wage determination in a multi-sector search-and-matching model. Specifically, Jackman and Roper is postulated as follows:

$$u \approx \frac{s}{\bar{f}} + s\frac{\sigma_f^2}{\bar{f}^3}. \tag{2.1}$$

[1] **?** adopts the measure of Neumann and Topel [1991] for the empirical investigation of wage Phillips curve.

where u is unemployment rate, s is the separation rate, $\bar{f}$ is the mean job-finding rate, and σ_f^2 is the cross-sectional variance of job-finding rates. This condition shows that the unemployment rate can rise because of the increased dispersion of job-finding probabilities across individuals even without changes in the mean separation and job-finding probability.[2] In this set-up, the separation rate is small and considered largely constant.[3]

The intuition is as follows. Workers with very low job-finding rates remain unemployed for extended periods. Even if most workers find jobs quickly, a small group with very low f_i can generate long unemployment durations and elevate structural unemployment. In this sense, aggregate unemployment depends critically on the left tail of the distribution of job-finding probabilities.[4] Since the job-finding probability is a function of market tightness, this condition implies that dispersion in job-finding probabilities—and, by extension, in market tightness—provides information about changes in structural unemployment.

Equation (2.1) suggests the following decomposition of changes in unemployment rate:

$$\Delta u \approx \underbrace{s\Delta\left(\frac{1}{\bar{f}_t}\right)}_{\text{mean job-finding change}} + \underbrace{s\Delta\left(\frac{\sigma_{f,t}^2}{\bar{f}_t^3}\right)}_{\text{dispersion in } f_i} + \underbrace{s\sum_i \Delta\omega_i \frac{1}{f_{i,t}}}_{\text{composition shifts}}.$$

2.2 Heterogeneity in the likelihood of separation and reallocation pressure

Separation heterogeneity Let aggregate unemployment be

$$u_t = \sum_i \omega_{i,t} u_{i,t}, \qquad u_{i,t} = \frac{s_{i,t}}{s_{i,t} + f_{i,t}},$$

where $\omega_{i,t}$ denotes the labor-force share of group i, $s_{i,t}$ its separation rate, and $f_{i,t}$ its job-finding rate. Define

$$\bar{s}_t = \sum_i \omega_{i,t} s_{i,t}, \qquad \bar{f}_t = \sum_i \omega_{i,t} f_{i,t},$$

[2] Details of the derivation are found in the appendix.
[3] This assumption is arguable, and we revisit this assumption in the extension.
[4] This result follows from Jensen's inequality.

and the cross-sectional second moments

$$\begin{aligned}
\mathsf{Var}_t(s_i) &= \sum_i \omega_{i,t}(s_{i,t} - \bar{s}_t)^2, \\
\mathsf{Var}_t(f_i) &= \sum_i \omega_{i,t}(f_{i,t} - \bar{f}_t)^2, \\
\mathsf{Cov}_t(s_i, f_i) &= \sum_i \omega_{i,t}(s_{i,t} - \bar{s}_t)(f_{i,t} - \bar{f}_t).
\end{aligned}$$

Then, up to a second-order approximation,

$$\Delta u_t \approx \underbrace{\Delta\left(\frac{\bar{s}_t}{\bar{s}_t + \bar{f}_t}\right)}_{\text{mean transition-rate effect}} + \underbrace{\Delta\left(\frac{-\bar{f}_t \mathsf{Var}_t(s_i) + \bar{s}_t \mathsf{Var}_t(f_i) + (\bar{s}_t - \bar{f}_t)\mathsf{Cov}_t(s_i, f_i)}{(\bar{s}_t + \bar{f}_t)^3}\right)}_{\text{dispersion effect}} + \underbrace{\sum_i \Delta\omega_{i,t} \frac{s_{i,t}}{s_{i,t} + f_{i,t}}}_{\text{composition effect}},$$

where $\Delta u_t = u_{t+1} - u_t$ and $\Delta\omega_{i,t} = \omega_{i,t+1} - \omega_{i,t}$.

Decomposition of the dispersion effect. Define the dispersion component as

$$D_t \equiv \frac{-\bar{f}_t \mathsf{Var}_t(s_i) + \bar{s}_t \mathsf{Var}_t(f_i) + (\bar{s}_t - \bar{f}_t)\mathsf{Cov}_t(s_i, f_i)}{(\bar{s}_t + \bar{f}_t)^3}.$$

Then D_t can be decomposed into

$$D_t = D_t^{(s)} + D_t^{(f)} + D_t^{(sf)},$$

where

$$\begin{aligned}
D_t^{(s)} &\equiv -\frac{\bar{f}_t \mathsf{Var}_t(s_i)}{(\bar{s}_t + \bar{f}_t)^3}, \\
D_t^{(f)} &\equiv \frac{\bar{s}_t \mathsf{Var}_t(f_i)}{(\bar{s}_t + \bar{f}_t)^3}, \\
D_t^{(sf)} &\equiv \frac{(\bar{s}_t - \bar{f}_t)\mathsf{Cov}_t(s_i, f_i)}{(\bar{s}_t + \bar{f}_t)^3}.
\end{aligned}$$

Taking first differences yields

$$\Delta D_t = \Delta D_t^{(s)} + \Delta D_t^{(f)} + \Delta D_t^{(sf)}.$$

Hence, the full decomposition of the change in aggregate unemployment is

$$\Delta u_t \approx \underbrace{\Delta\left(\frac{\bar{s}_t}{\bar{s}_t+\bar{f}_t}\right)}_{\text{mean transition-rate effect}} + \underbrace{\Delta D_t^{(f)}}_{\text{job finding}} + \underbrace{\Delta D_t^{(s)}}_{\text{separations}} + \underbrace{\Delta D_t^{(sf)}}_{\text{covariance}} + \underbrace{\sum_i \Delta\omega_{i,t}\frac{s_{i,t}}{s_{i,t}+f_{i,t}}}_{\text{composition effect}}. \tag{2.2}$$

Interpretation. Equation (2.2) shows that the dispersion effect can itself be decomposed into three parts. The term $\Delta D_t^{(s)}$ captures the contribution of cross-group dispersion in separation rates, $\Delta D_t^{(f)}$ captures the contribution of cross-group dispersion in job-finding rates, and $\Delta D_t^{(sf)}$ captures the contribution of the covariance between the two transition rates.

The separation-dispersion term $D^{(s)}$ is negative because unemployment is concave in separation rates, and the sign of the covariance term $D^{(sf)}$ is ambiguous. Thus, dispersion in separation alone tends to reduce unemployment, but depending on the covariance term, the dispersion of separation can raise unemployment rate under two circumstances: (1) If high-separation groups also have high job-finding rates ($\mathrm{Cov}(s_i, f_i) > 0$), then both terms reduce unemployment; (2) If high-separation groups have low job-finding rates ($\mathrm{Cov}(s_i, f_i) < 0$), the covariance term raises unemployment and may dominate.

2.3 Role of AI in the dispersion of job-finding rates

We focus on the dispersion in job-finding rates, since the sum of $D^{(s)}$ and $D^{(sf)}$ has an ambiguous sign. The term $D^{(s)}$ is further decomposed into the portion attributable to AI and that to other factors (within-AI group dispersion).

The cross-sectional variance of job-finding rates among the unemployed admits the decomposition:

$$D_t^{(f)} = \mathrm{Var}_t\big(f_{it}\big) = \underbrace{\mathrm{Var}_t\big[E_a(f_{it}(a_{it}))\big]}_{\text{between-AI component}} + \underbrace{E_a\big[\mathrm{Var}_t\big(f_{it}(a_{it})\big)\big]}_{\text{within-AI component}}. \tag{2.3}$$

The first term on the right-hand side captures the **between-AI component**—that is, the dispersion attributable to differences in AI exposure—while the second term captures the **within-AI component**, reflecting dispersion arising from factors other than AI within groups that share

the same level of AI exposure. The above decomposition can also incorporate an additional dimension of observed heterogeneity. For example, with industry heterogeneity, it can be decomposed into a between-industry component, a within-industry between-AI component, and a within-industry within-AI component (the residual). Essentially, the same empirical framework can be applied to analyze dispersion arising from heterogeneous separation rates.

2.4 Implications for mismatch

Jackman and Roper [1987] describe the condition for optimal allocation as follows: the social planner aims to "equalize" market tightness or job-finding rates by reallocating workers from markets with fewer jobs and less efficient matching to those with more job openings and more efficient matching processes. It is because the dispersion increases because of allocative frictions that hamper effective reallocation of labor for the most productive use.

To measure the degree of mismatch, Şahin et al. [2014] state this condition based on a multi-sector model as follows (equation 1):

$$\phi_{it} m_{ui} \left(\frac{v_{it}}{u^*_{it}} \right) = \phi_{jt} m_{uj} \left(\frac{v_{jt}}{u^*_{jt}} \right) \quad \text{for} \quad i \neq j \tag{2.4}$$

where $\phi_{it} m_{ui}$ is sector-specific matching efficiency, m_{ui} is the derivative of matching function with respect to an unemployed worker in sector i, v_{it} is the number of vacancies in sector i, and u^*_{it} is the optimal number of unemployed workers—the social planner's allocation.

In this set up, the mismatch index is written as:

$$M_{\phi,t} = 1 - \frac{h_t}{h^*_t} = 1 - \sum_{i=1}^{I} \left(\frac{\phi_{it}}{\bar{\phi}_t} \right) \left(\frac{v_{it}}{v_t} \right)^{\alpha} \left(\frac{u_{it}}{u_t} \right)^{1-\alpha},$$

where α (1-α) is the elasticity of vacancies (unemployed workers) in a CRS matching function and $\bar{\phi}_t$ is a CES aggregator of the sector-level matching efficiencies weighted by their vacancy share.

$$\bar{\phi}_t = \left[\sum_{i=t}^{I} \phi_{it}^{1/\alpha} \left(\frac{v_{it}}{v_t} \right) \right]^{\alpha}$$

It is important to note that the larger the dispersion of market tightness is, the smaller the second term of equation (2.4) because of the convexity of the CRS matching function, thereby

producing a higher index of mismatch. In this sense, the mismatch index essentially reflects the cross-sectional dispersion of job-finding rates or market tightness, inheriting the original idea of equation (2.1).

This result suggests the dispersion in job-finding rates measures the degree of mismatch, and our framework (2.3) further allows the mismatch into the components attributable to AI and non-AI factors.

It is important to note that this theoretical framework applies not only to unemployed workers actively searching for jobs, but also to the job-finding prospects of those already employed in sector i and those out of the labor force who seek employment in sector i. In this way, the framework also captures the effects of reallocation frictions on labor supply and job-to-job transitions, which we will elaborate further in Section 7.

3 Data

We combine microdata from the Current Population Survey with information on occupations' AI exposure, demand for AI-related skills, and vacancy counts.

3.1 AI exposure and adoption

AI exposure We obtain our preferred measure of an occupation's exposure to AI from Eloundou et al. [2023], which we refer to as OpenAI exposure scores throughout this paper. This ranking was constructed by labeling direct work activities and task descriptions from the Occupational Information Network (O*NET) based on an assessment of whether access to an LLM or LLM-powered system would reduce the time required to complete the activity or task by at least 50% without loss of quality. We use the authors' GPT-4 assigned β exposure measure, which considers the use of complementary tools or software on top of LLMs. Occupation-level exposure scores are averages over task-level exposure, where supplemental O*NET tasks are assigned half the weight of core tasks.

In robustness checks, we use an alternative measure of AI exposure based on data from the Anthropic Economic Index [Handa et al., 2025]. This dataset provides descriptions of hundreds of distinct AI applications derived from millions of prompts submitted to Claude. For each AI

application (e.g. "develop time series forecasting models"), we convert the text to a numerical word embedding and do same for each O*NET task description. Following [Hampole et al., 2025], we consider a task exposed to AI if the cosine similarity between the task embedding and *any* AI application embedding is above the 95th percentile of similarity across all task-application pairs. We then aggregate task-level expose to occupations as described above. Beyond providing an independent measure of AI exposure, the Anthropic data also allow us to distinguish between applications that primarily automate versus augment human labor based on user interaction patterns identified by Anthropic.

AI adoption Both the OpenAI and Anthropic exposure scores capture the extent to which generative AI applications might *feasibly* perform the same tasks as a human worker. However, the degree to which AI is actually being used to accomplish exposed tasks varies considerably across occupations and has risen over time as the underlying technology has improved. We therefore supplement our AI exposure scores with a measure of AI utilization constructed from online job postings. Using data from Lightcast, we compute the share of job postings that mention an AI-related skill requirement for each occupation and month. We consider a position to be utilizing AI if Lightcast tags it with a skill that includes the terms "artificial intelligence" or "machine learning" in its description.

3.2 Current Population Survey

We assign each individual in the CPS an AI exposure based on their reported occupation and the indices defined in Section 3.1. When CPS occupation categories include more than one detailed O*NET occupation, we use their average exposure score. We additionally harmonize CPS occupations—which were revised to reflect the 2018 Standard Occupational Classification starting in 2020:M1—to definitions that are fully comparable from 2011:M1 to 2025:M12.

Individuals without prior work experience—such as young labor force entrants—are missing occupational information and therefore cannot be assigned an occupation-based AI exposure. Yet it is precisely these workers who may be most affected by AI [Brynjolfsson et al., 2025a]. We therefore we impute the AI-exposure score for individuals who do not report an occupation using

the average exposure of other individuals with the same gender, age, and education.[5] This allows us to define exposure for the full population, a necessary step when studying macroeconomic aggregates. AI exposure ranges from 0 (no exposure) to 1 (full exposure), similar to a probability. By multiplying the score (and one minus the score) by the individual sampling weight, we construct stocks and flows for fully exposed (high-exposure) and non-exposed (low-exposure) workers. This approach preserves accounting identities for stocks and flows within exposure groups and in the aggregate.

3.3 Vacancies

We compute vacancies by occupation using data from the Job Openings and Labor Turnover Survey (JOLTS) and Lightcast. We start with the level of JOLTS openings by 2-digit industry i in month t, denoted V_{it}. Because JOLTS does not contain information on occupations, we allocate industry-level openings to occupations in proportion to share of Lightcast job postings for occupation o in industry i, denoted L_{oit}. Finally, we sum across industries to recover the count of vacancies by occupation,

$$V_{ot} = \sum_{i \in I} \frac{L_{oit}}{\sum_{o \in O} L_{oit}} \times V_{it}^{JOLTS}. \tag{3.1}$$

This imputation produces a series of vacancies by occupation that is fully consistent with level of job openings from JOLTS when aggregated.

4 Demographics of AI exposure

This section examines heterogeneity in AI exposure across demographic groups, education levels, and industries.

Table 1 reports average AI exposure across demographic groups, education levels, and industries using two alternative measures based on OpenAI and Anthropic classifications. A consistent pattern across all categories is that the Anthropic measure yields higher exposure levels than the OpenAI measure, although the relative rankings across groups are broadly similar. This suggests

[5] We further consider cohort, but this extension does not change the result materially.

that while the level of exposure differs across measures, the cross-sectional heterogeneity is robust.

Across demographic groups, women exhibit higher AI exposure than men under both measures. The difference is modest but consistent, indicating that occupations with higher AI exposure are slightly more concentrated among female workers. Across age groups, exposure increases with age: younger workers (ages 16–24) have substantially lower exposure, while prime-age and older workers exhibit similar and higher levels of exposure. This pattern likely reflects the occupational distribution of younger workers, who are more concentrated in roles less exposed to AI technologies.

Educational attainment is strongly positively associated with AI exposure. Workers with less than a high school education have the lowest exposure, while college graduates have the highest exposure by a wide margin. For example, exposure among college graduates is more than twice that of workers without a high school degree under both measures. This gradient highlights that AI exposure is concentrated in more skill-intensive occupations, consistent with the idea that current AI technologies are more applicable to cognitive and analytical tasks.

There is also substantial heterogeneity across industries. Figure 1 summarizes the AI exposure by industry. Sectors such as retail, professional services, finance, and public administration exhibit relatively high levels of AI exposure, while agriculture, construction, and leisure and hospitality display much lower exposure. Notably, retail shows the highest exposure under both measures, which may reflect the growing role of AI in customer service, logistics, and inventory management. Similarly, professional and financial services exhibit high exposure, consistent with the use of AI in information processing and decision-making tasks. In contrast, industries that rely more heavily on manual or in-person tasks tend to have lower exposure.

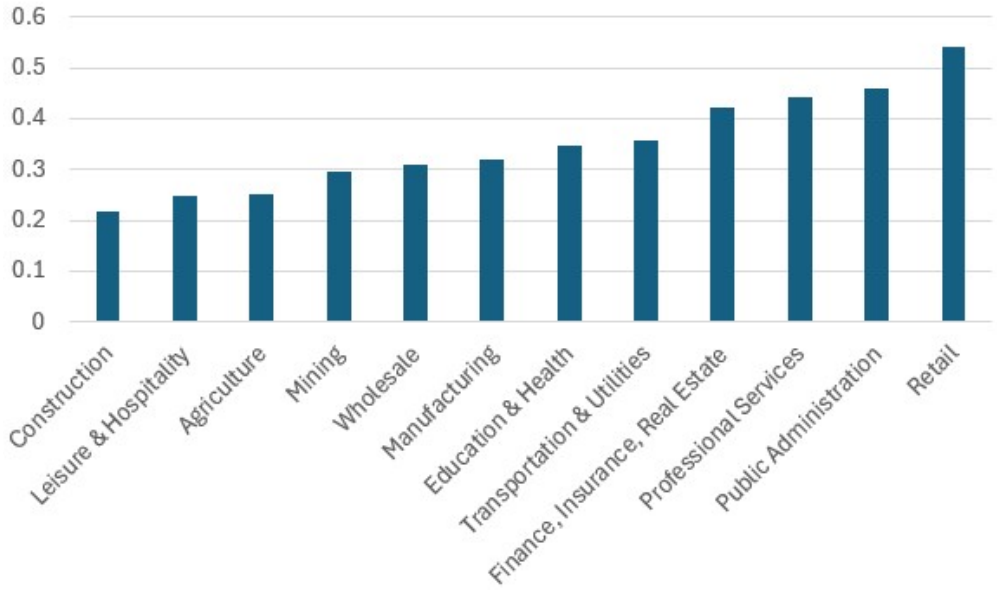
Overall, the results indicate that AI exposure is unevenly distributed across the labor market, with higher exposure concentrated among more educated workers and in service-oriented, information-intensive industries. These patterns suggest that the diffusion of AI is likely to have heterogeneous effects across workers and sectors, with important implications for labor reallocation and inequality.

Table 1: AI EXPOSURE BY DEMOGRAPHIC AND INDUSTRY GROUP

	OpenAI	Anthropic
Gender		
Men	0.31	0.56
Women	0.37	0.59
Age		
16–24	0.25	0.46
25–54	0.35	0.60
55+	0.36	0.59
Education		
Less than high school	0.19	0.40
High-school graduation	0.29	0.50
Some college & associate degree	0.35	0.57
College graduation	0.44	0.73
Industry		
Agriculture	0.25	0.42
Mining	0.30	0.54
Construction	0.22	0.49
Manufacturing	0.32	0.56
Transportation & Utilities	0.36	0.57
Wholesale	0.31	0.53
Retail	0.54	0.75
Finance, Insurance, Real Estate	0.42	0.66
Professional Services	0.44	0.67
Education & Health	0.35	0.67
Leisure & Hospitality	0.25	0.46
Public Administration	0.46	0.66

Notes: Entries report time-average exposure shares for OpenAI and Anthropic measures.

Figure 1: AI EXPOSURE BY INDUSTRY



Note: This bar chart displays the AI exposure by industry based on the OpenAI's AI exposure measure.
Source: Authors' calculation.

5 Disparities in stocks and flows by AI exposure

This section documents disparities in labor market outcomes by AI exposure and adoption. Section 5.1 discusses stocks and flows by AI exposure. Section 5.4 documents the market tightness by AI exposure and adoption.

5.1 Measurement of stocks and flows by AI exposure

Stock of labor force status Let x_{it}^o denote the AI exposure of individual i, whose occupation is o, at time t. If individual i is employed, we observe their current occupation; if unemployed, we observe their previous occupation. Note that x_{it}^o is a probability taking values between 0 and 1, capturing the degree of AI exposure, while $1 - x_{it}^o$ captures the degree of AI non-exposure.

The total number of individuals employed and unemployed by the AI exposure is computed from the following. Let E_t be the number of employed individuals at time t:

$$E_t = \sum_{i=1}^{N} w_{it} \mathbf{1}(l_{it} = E), \tag{5.1}$$

where w_{it} is the weight of individual i at t and $\mathbf{1}(l_{it} = E)$ is the indicator that takes the value 1 when individual i's labor force status (l_{it}) is employed (E).

The number of employed individuals with AI exposure (E_t^x) and without AI exposure (E_t^{nx}) is computed from the following:

$$E_t^x = \sum_{i=1}^{N} w_{it} x_{it} \mathbf{1}(l_{it} = E) \tag{5.2}$$

$$E_t^{nx} = \sum_{i=1}^{N} w_{it} (1 - x_{it}) \mathbf{1}(l_{it} = E). \tag{5.3}$$

Likewise, the number of unemployed individuals with and without AI exposure, U_t^x and U_t^{nx} respectively, is written as:

$$U_t^x = \sum_{i=1}^{N} w_{it} x_{it} \mathbf{1}(l_{it} = U) \tag{5.4}$$

$$U_t^{nx} = \sum_{i=1}^{N} w_{it} (1 - x_{it}) \mathbf{1}(l_{it} = U), \tag{5.5}$$

where U denotes the unemployment status. Note that the sum of U_t^x and U_t^{nx} equates U_t.

The level of labor force exposed to AI or not is expressed as:

$$L_t^x = E_t^x + U_t^x \tag{5.6}$$

$$L_t^{nx} = E_t^{nx} + U_t^{nx}. \tag{5.7}$$

Now we can compute the unemployment rate of workers exposed and non-exposed to AI, each denoted by u_t^x and u_t^{nx}, is computed from:

$$u_t^x = \frac{U_{it}^x}{L_{it}^x} \times 100, \qquad u_t^{nx} = \frac{U_{it}^{nx}}{L_{it}^{nx}} \times 100. \tag{5.8}$$

For nonparticipation, an individual's information on AI exposure is limited, unless the individual was either previously employed or unemployed. We take the most recent (or near future) AI exposure as a proxy for the AI exposure during the nonparticipation spell. In this context, the

number of individuals out of the labor force, each denoted by N_t^x and N_t^{nx}, is expressed as:

$$N_t^x = \sum_{i=1}^{N} w_{it} x_{it} \mathbf{1}(l_{it} = N) \tag{5.9}$$

$$N_t^{nx} = \sum_{i=1}^{N} w_{it} (1 - x_{it}) \mathbf{1}(l_{it} = N), \tag{5.10}$$

where N denotes the nonparticipation status.

The number of civilian population exposed and not exposed to AI, denoted by P_t^x and P_t^{nx}, respectively, is

$$P_t^x = E_t^x + U_t^x + N_t^x \tag{5.11}$$

$$P_t^{nx} = E_t^{nx} + U_t^{nx} + N_t^{nx}. \tag{5.12}$$

Accordingly, the labor force participation rate with and without the AI exposure (l_t^x and l_t^{nx}, respectively) and the employment-to-population ratio with and without the AI exposure (e_t^x and e_t^{nx}, respectively) are written as follows:

$$l_t^x = \frac{L_{it}^x}{P_{it}^x} \times 100, \qquad l_t^{nx} = \frac{L_{it}^{nx}}{P_{it}^{nx}} \times 100 \tag{5.13}$$

$$e_t^x = \frac{E_{it}^x}{P_{it}^x} \times 100, \qquad e_t^{nx} = \frac{E_{it}^{nx}}{P_{it}^{nx}} \times 100. \tag{5.14}$$

Labor market flows Next, we construct labor market flow rates across employment (E), unemployment (U), and nonparticipation (N), separately for the AI-exposed and non-exposed workers. Let $l_{it} \in E, U, N$ denote individual i's labor force status at time t. For example, the level of flows from E in $t-1$ to U in t of workers exposed to AI is

$$f_t^x(E \to U) = \sum_{i=1}^{N} \tilde{w}_{it}, x_{it}, \mathbf{1}(l_{i,t-1} = E, l_{it} = U), \tag{5.15}$$

where $\tilde{w}_{it}$ is the individual weight for matched flows data from IPUMS. Analogously for the non-exposed component,

$$f_t^{nx}(E \to U) = \sum_{i=1}^{N} w_{it}, (1 - x_{it}), \mathbf{1}(l_{i,t-1} = E, l_{it} = U). \tag{5.16}$$

Flow rates are obtained by normalizing these gross flows by the corresponding origin stocks. For example, the employment-to-unemployment transition rate among AI-exposed workers (EU) is given by

$$\text{EU}_t^x = \frac{f_t^x(E \to U)}{f_t^x(E \to E) + f_t^x(E \to U) + f_t^x(E \to N)}. \tag{5.17}$$

Let $\tilde{E}_{t-1}^x = f_t^x(E \to E) + f_t^x(E \to U) + f_t^x(E \to N)$ and $\tilde{E}_{t-1}^{nx} = f_t^{nx}(E \to E) + f_t^{nx}(E \to U) + f_t^{nx}(E \to N)$. The analogous definition of non-exposed workers is written as follows:

$$\text{EU}_t^{nx} = \frac{f_t^{nx}(E \to U)}{\tilde{E}_{t-1}^{nx}}. \tag{5.18}$$

The EN rate is computed as follows:

$$\text{EN}_t^x = \frac{f_t^x(E \to N)}{\tilde{E}_{t-1}^x} \qquad \text{EN}_t^{nx} = \frac{f_t^{nx}(E \to N)}{\tilde{E}_{t-1}^{nx}}. \tag{5.19}$$

Likewise, the UE and UN rates of workers exposed to and non-exposed to AI are written as follows:

$$\text{UE}_t^x = \frac{f_t^x(U \to E)}{\tilde{U}_{t-1}^x} \qquad \text{UE}_t^{nx} = \frac{f_t^{nx}(U \to E)}{\tilde{U}_{t-1}^{nx}} \tag{5.20}$$

$$\text{UN}_t^x = \frac{f_t^x(U \to N)}{\tilde{U}_{t-1}^x} \qquad \text{UN}_t^{nx} = \frac{f_t^{nx}(U \to N)}{\tilde{U}_{t-1}^{nx}}. \tag{5.21}$$

Finally, transitions originating from nonparticipation are summarized by the NE and NU rates, defined as follows:

$$\text{NE}_t^x = \frac{f_t^x(N \to E)}{\tilde{N}_{t-1}^x} \qquad \text{NE}_t^{nx} = \frac{f_t^{nx}(N \to E)}{\tilde{N}_{t-1}^{nx}} \tag{5.22}$$

$$\text{NU}_t^x = \frac{f_t^x(N \to U)}{\tilde{N}_{t-1}^x} \qquad \text{NU}_t^{nx} = \frac{f_t^{nx}(N \to U)}{\tilde{N}_{t-1}^{nx}} \tag{5.23}$$

$$\tag{5.24}$$

Rates of jobs and activities switches We further construct rates of switching establishments and activity switching within an establishment between $t-1$ and t. Let JJ_t^x and JJ_t^{nx} denote the rate of job-to-job transitions at time t among AI-exposed and non-exposed workers, respectively. Let AA_t^x and AA_t^{nx} denote the rate of within-establishment activity switches at time t for AI-

Table 2: MEAN LABOR MARKET INDICATORS OF STOCKS AND FLOWS (2011:M1-2026:M1, %)

	[A] UR	[B] LFPR	[C] EPOP	[D] EU	[E] UE	[F] EN	[G] NE	[H] NU	[I] UN
All	5.4	62.8	59.3	1.2	24.2	3.1	4.2	2.1	24.5
High AI	4.3	64.6	61.8	0.9	22.6	2.8	3.9	1.7	25.2
Low AI	6.0	61.8	58.0	1.4	24.8	3.3	4.4	2.3	24.2

Note: Columns [D]–[I] report the average monthly transition rates.
Source: Authors' calculation.

exposed and non-exposed workers, respectively. Note that both rates are normalized by the corresponding matched employment stocks, $\tilde{E}^{x}_{t-1}$ and $\tilde{E}^{nx}_{t-1}$.

The estimates, JJ^{x}_{t}, JJ^{nx}_{t}, AA^{x}_{t} and AA^{nx}_{t}, are computed as follows. Let E' denote the status of employment at a new job (establishment), A denote the status of employment with the same activity as the previous one, and A' denote the status of employment with a new activity at the same job (establishment):

$$\text{JJ}^{x}_{t} = \frac{f^{x}_{t}(E \to E')}{\tilde{E}^{x}_{t-1}} \qquad \text{JJ}^{nx}_{t} = \frac{f^{nx}_{t}(E \to E')}{\tilde{E}^{nx}_{t-1}} \tag{5.25}$$

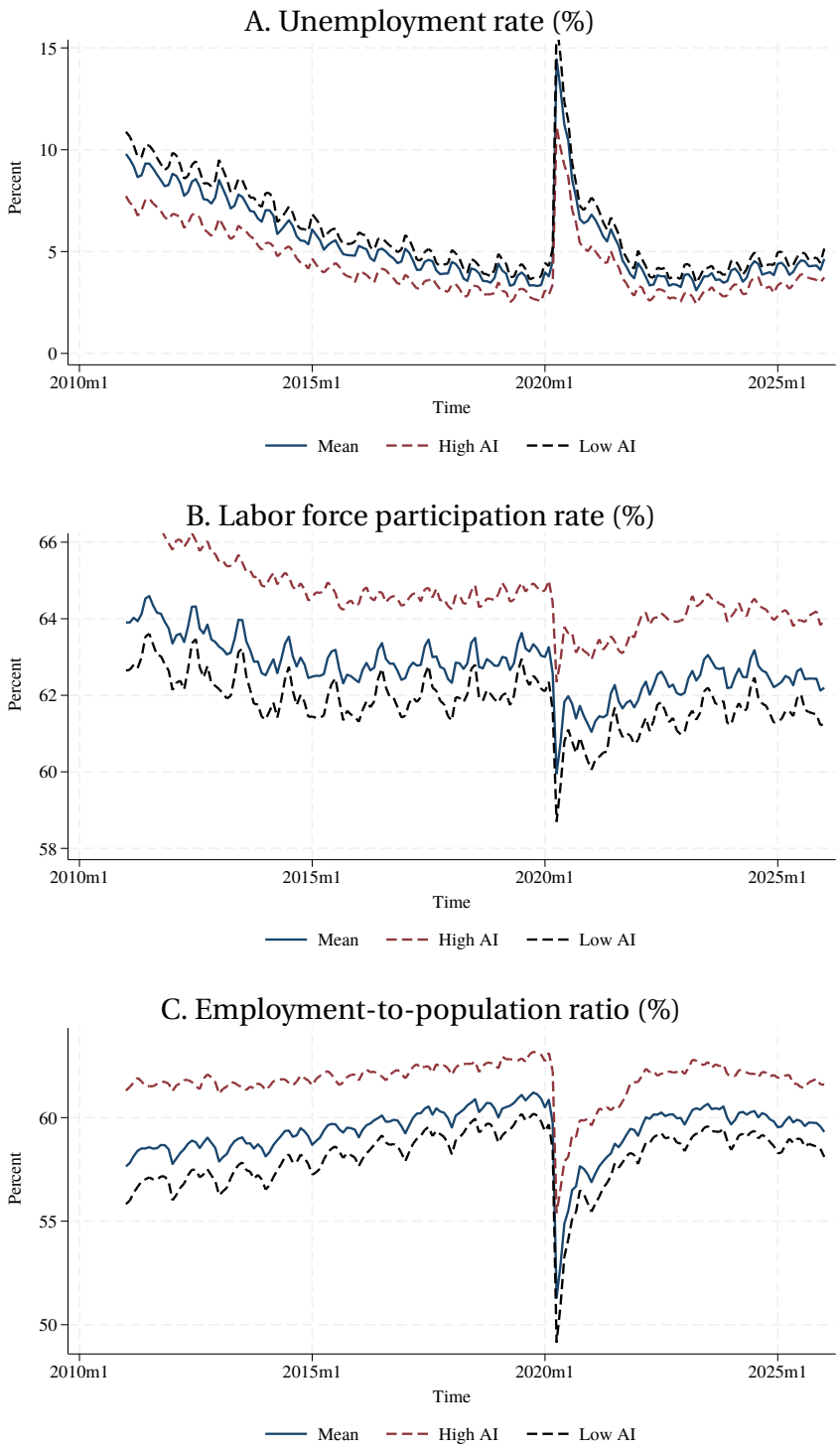
$$\text{AA}^{x}_{t} = \frac{f^{x}_{t}(A \to A')}{\tilde{E}^{x}_{t-1}} \qquad \text{AA}^{nx}_{t} = \frac{f^{nx}_{t}(A \to A')}{\tilde{E}^{nx}_{t-1}}. \tag{5.26}$$

5.2 Stock and Flows by the AI exposure

This section reports the estimated stocks, flows and labor-market outcomes for AI-exposed and non-exposed workers. Table 2 summarizes these statistics.

Unemployment rate Figure 2 displays u^{x}_{t} and u^{nx}_{t} together with the aggregate unemployment rate (u_t). Consistent with u^{x}_{t} lying below u^{nx}_{t}, AI-exposed workers have a lower unemployment rate than non-exposed workers. Over 2011:M1–2025:M9, the average unemployment rate is 5.5%, compared with 4.0% for AI-exposed workers and 6.3% for non-exposed workers. This gap is primarily driven by a lower EU rate and a higher UE rate among AI-exposed workers relative to their non-exposed counterparts (Panels A and E of Figure 4). In other words, AI-exposed workers are less likely to separate from employment and more likely to transition into employment when unemployed. At the same time, AI-exposed workers are more likely to re-enter unemployment from nonparticipation and less likely to exit the labor force when unemployed, which exerts

Figure 2: UNEMPLOYMENT RATE AND EPOP RATIO WITH/WITHOUT AI EXPOSURE



Note to figure: Panels A, B, and C show the unemployment rate, LFPR and EPOP ratio for all workers (thick blue line), AI-exposed workers (solid red line), and AI non-exposed workers (dashed black line), respectively. AI exposure is measured using OpenAI's occupation-level estimates.

Source: Authors' calculation

Figure 3: SHARE OF AI-EXPOSED WORKERS IN THE LABOR FORCE AND POPULATION



Note to figure: This figure shows the share of individuals in the labor force and population exposed by AI. AI exposure is measured using OpenAI's occupation-level estimates.
Source: Authors' calculation

upward pressure on their unemployment rate. Nevertheless, because the net effects of UE and EU flows dominate those of UN and NU flows (Panels B and D of Figure 4), AI exposure lowers the unemployment rate on net.

It is also important to note that AI-exposed workers exhibit stronger attachment to the labor force. Specifically, NU and NE flows are an order of magnitude higher among AI-exposed workers than among non-exposed workers (Panels B and E of Figure 4). By contrast, EN and UN flows are an order of magnitude higher for non-exposed workers (Panels C and D of Figure 4). Taken together, these patterns imply that AI-exposed workers are less likely to exit the labor force and more likely to re-enter it once out of the labor force.

Labor force participation rate and employment-to-population ratio Panel B displays l_t^x and l_t^{nx} together with the aggregate labor force participation rate (l_t), and panel C displays e_t^x and e_t^{nx} together with the aggregate employment-to-population ratio (e_t). Since the employment-to-population ratio (EPOP ratio, henceforth) reflects both the labor force participation rate (LFPR, henceforth) and the unemployment rate, we focus on the EPOP ratio.

Consistent with e_t^x lying above e_t^{nx}, AI-exposed workers exhibit a higher EPOP ratio than non-exposed workers. Over 2011:M1–2025:M9, the average EPOP ratio is 58.7%, compared with 95.1% for AI-exposed workers and 48.3% for non-exposed workers. In other words, AI-

exposed workers are less likely to exit the labor force upon leaving employment and more likely to transition back into employment from nonparticipation. Moreover, they are less likely to give up job search when unemployed and more likely to resume job search when out of the labor force, and conditional on searching, they experience higher job-finding probabilities. Together, these patterns contribute to the higher EPOP ratio among AI-exposed workers.

Shares of AI-exposed workers in non-employment With the UE and NE rates, we can back out shares of workers exposed to AI in the following way:

$$UE_t = w^x UE_t^x + (1 - w^x) UE_t^{nx} \tag{5.27}$$

$$NE_t = \chi^x NE_t^x + (1 - \chi^x) NE_t^{nx}, \tag{5.28}$$

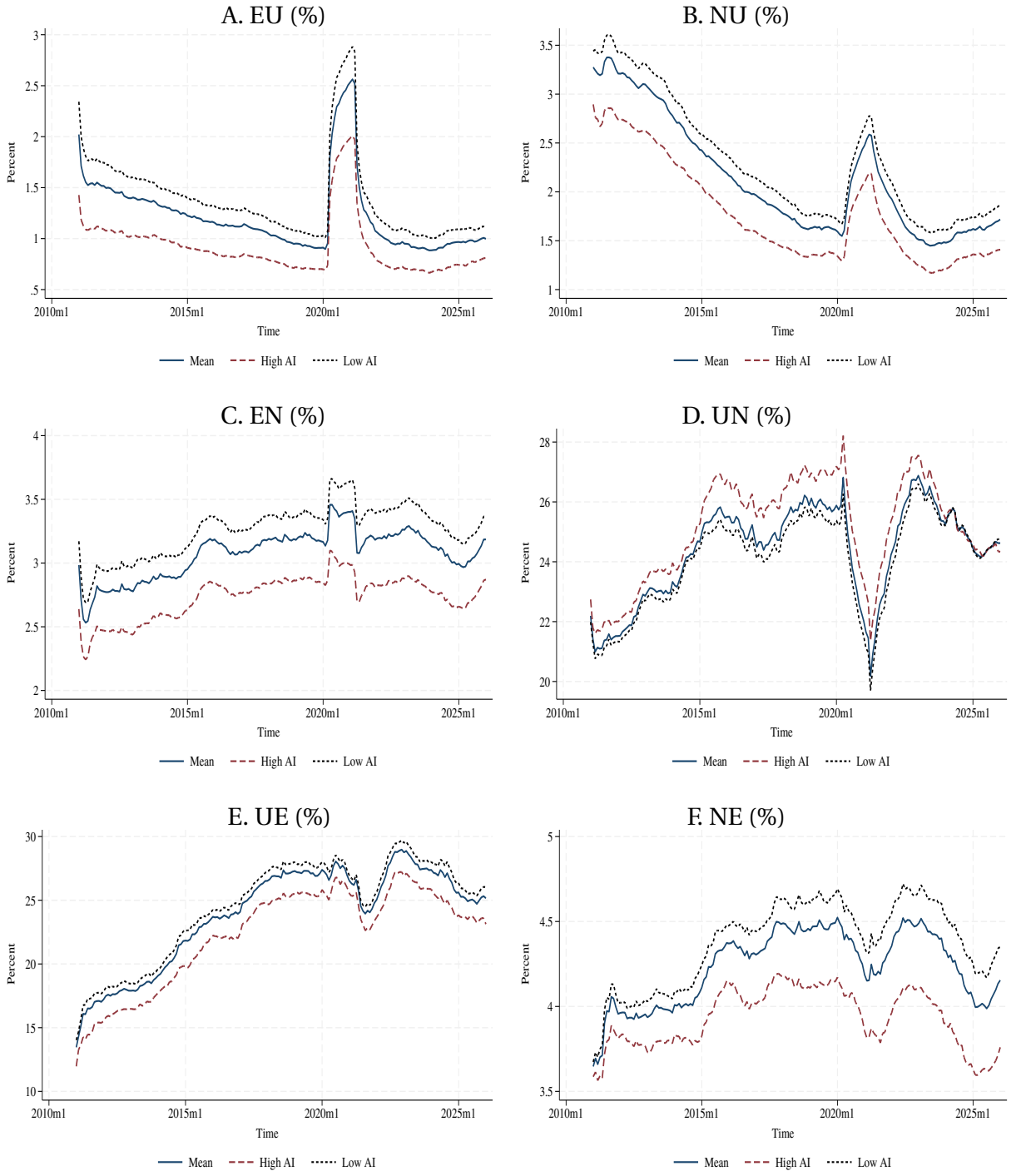
where w^x and χ^x are the shares in unemployment and nonparticipation, respectively. Since we observe the flows rates of both sides, we can back out the unobserved shares.

Panels G and H of Figure 4 display w^x and χ^x, respectively. The share of AI-exposed workers in unemployment hovers around 20% prior to the pandemic and spikes during the COVID-19 recession. It subsequently returns to its pre-pandemic level before gradually increasing from 2023 onward. This post-2022 uptrend likely reflects increased job search activity among AI-exposed workers and their reallocation. Meanwhile, the share of AI-exposed workers in nonparticipation remains broadly flat at about 2.25 percentage points, except during the pandemic recession.

AI's effects on the worker reallocation So far, we have examined six different flow rates. To provide a comprehensive measure of worker reallocation and its magnitude, we compute the fraction of all six labor force status transitions between $t-1$ and t relative to the civilian noninstitutional population at $t-1$, which we refer to as the worker reallocation rate.

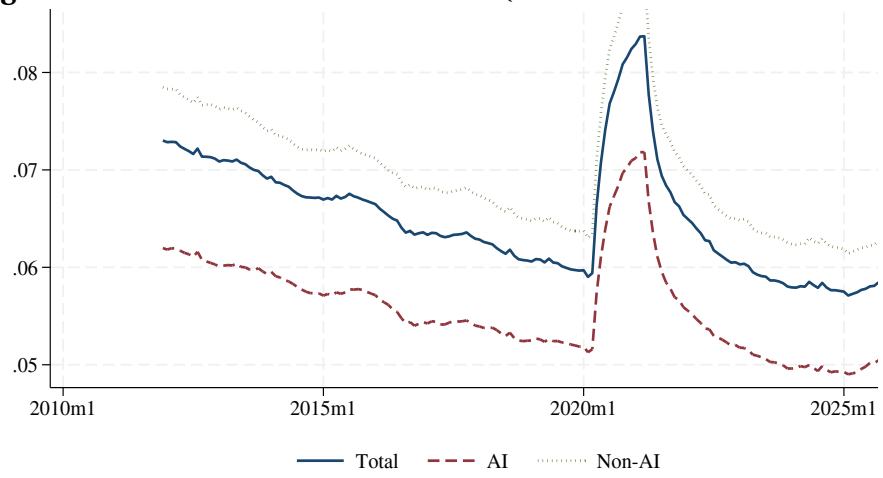
Figure 7 displays the worker reallocation rate by AI exposure. In general, workers with low AI exposure are more likely to switch labor force status than those with high AI exposure, consistent with greater job instability among low-exposure workers. Following the Great Recession, overall reallocation declined steadily, spiked during the COVID-19 pandemic, and then resumed its downward trend. This pattern is evident for both high- and low-exposure groups, suggesting a broad-based decline in reallocation activity in the U.S. labor market over time. Notably, however,

Figure 4: LABOR FLOWS BY AI EXPOSURE (12-MONTH MOVING AVERAGE)



Note to figure: Panel A displays the E-to-U flows rate for all workers (thick blue line), AI-exposed workers (solid red line), and AI non-exposed workers (dashed black line). The remaining panels report the flow rates indicated in each panel title for the same groups. Panels G and H display the share of workers exposed to AI in the unemployment and nonparticipation pool, respectively. AI exposure is measured using OpenAI's occupation-level estimates.
Source: Authors' calculation

Figure 5: WORKER REALLOCATION RATE (12-MONTH MOVING AVERAGE)



Note to figure: This figure displays the worker reallocation rate by AI exposure. The solid blue line shows the average reallocation rate; the red dashed line represents the reallocation rate for workers with high AI exposure; and the dotted black line represents the reallocation rate for workers with low AI exposure.
Source: Authors' calculation

the decline in reallocation appears to have stabilized around 2024 and begun to rise again in 2025, potentially reflecting the growing impact of AI.

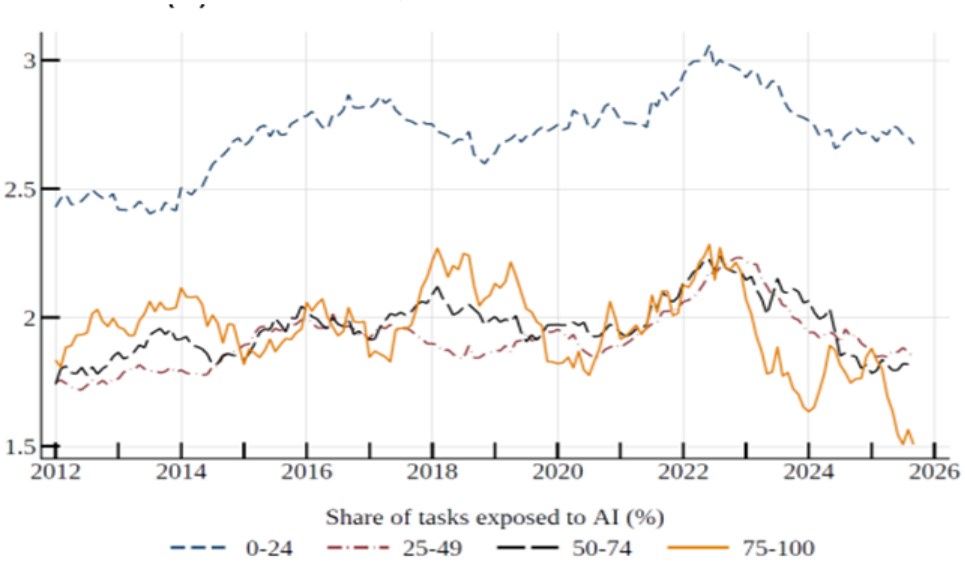
Switches of employers and job activities Figure 6 presents the job-switch rate (Panel A) and the activity-switch rate (Panel B) by AI exposure. The CPS asks respondents whether they, if employed in two consecutive months, changed employer since last month, which is used to compute the job-to-job transition rate. The CPS also asks respondents who have not changed employer whether they experienced changes in their work activities, which is used to compute the activity switch rate.

We group workers into bins based on the share of their current occupation's tasks exposed to AI. For example, the 75-100% bin contains around 20 occupations, but these make up less than 25% of total employment. Instead of using employment-weighted quartiles, we adopt this approach because AI may have had particularly large effects on changes in within-job activities and job switches among the most exposed occupations such as software developers, telemarketers, and various clerical workers. In addition, we plot 12 month moving averages to smooth through some of the month-to-month noise and to handle seasonality.

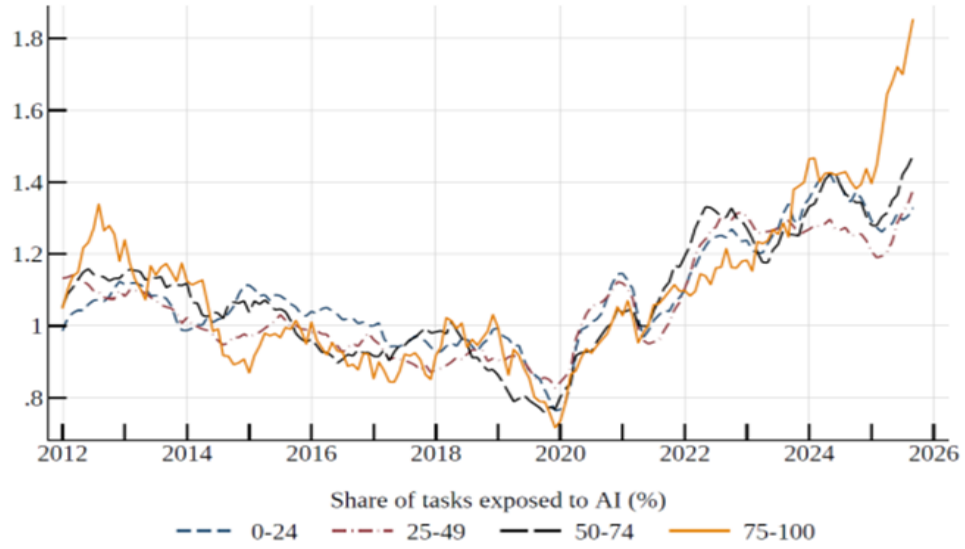
The job-to-job transition rate is about 0.5 percentage point higher in occupations with an

Figure 6: SWITCHES OF JOBS AND ACTIVITIES BY AI EXPOSURE

A. Job-to-job transition rate (%)



B. Activity-switch rate (%)



Note to figure: Panels A and B display the job-switch rate and activity-switch rate by AI exposure. For AI exposure, we use the share of tasks exposed to AI based on OpenAI's occupation-level estimates.
Source: Authors' calculation

AI-exposed task share of 25 percent or less than in other occupations. Meanwhile, the job-switch rates of the other groups are broadly similar. Given that low AI exposure occupations tend to be lower skilled, this pattern is consistent with the evidence that job-to-job transitions are more frequent among workers in low-skilled or less stable jobs (Ahn et al., 2023).

Notably, the job-to-job transition rate declined a bit more rapidly among the highest-exposure group, defined as occupations with an AI-related task share of 75 percent or higher. This pattern likely reflects relatively weaker labor demand for these workers compared with other groups, following the introduction of LLMs in late 2022. Job-to-job transition rates do not appear to indicate increased reallocation activity at the margin.

The activity-switch rate paints a markedly different picture of AI's reallocation effects. Across the four exposure groups, activity-switch rates are similar through 2024. However, starting around 2025, the highest-exposure group exhibits a much faster increase in activity-switch rates than the other groups. This pattern suggests that reallocation is increasingly concentrated within establishments and within current jobs.

Overall, the evidence suggests that AI has not led to increased reallocation through job-to-job transitions but has instead reshaped adjustment along the intensive margin within jobs. While job-switch rates show little evidence of increased reallocation—and even decline for the highest-exposure group-activity-switch rates rise disproportionately for that group, suggesting that reallocation is increasingly concentrated within establishments through changes in job tasks.

5.3 Worker flows by AI exposure and adoption

With the transition data, we construct worker reallocation flows by AI exposure. To assess the effects of AI on worker reallocation flows, we first sort industries into bins based on their AI exposure from OpenAI and AI adoption from Lightcast in each quarter. We form terciles of AI exposure and split AI adoption into high and low groups using the within-quarter median, yielding six groups (e.g., low exposure/low adoption, high exposure/high adoption). We then compute the mean worker reallocation measures for each group.

Figure 7 presents worker reallocation measures analogous to job reallocation. Job-finding reallocation (Panel A) captures the share of U-to-E and N-to-E transitions relative to the civilian

noninstitutional population, while job-loss reallocation (Panel B) captures the share of E-to-U and E-to-N transitions. Total reallocation aggregates all six transitions, including UN and NU flows.

Overall, worker churn—particularly along the job-finding margin—is more pronounced among low AI-exposure workers, consistent with negative effects of AI exposure on the job-finding rate observed in the flow data. Meanwhile, higher AI adoption is generally associated with reduced reallocation activity along both the job-finding and job-loss margins, while effects of AI adoption is mixed in job reallocation. This observation suggests that higher AI exposure and adoption are characteristic of more stable, high-skilled jobs, leading to lower worker churn. A similar pattern is observed in job flows including job destruction and job creation, documented in the appendix.

5.4 Market tightness by AI exposure and adoption

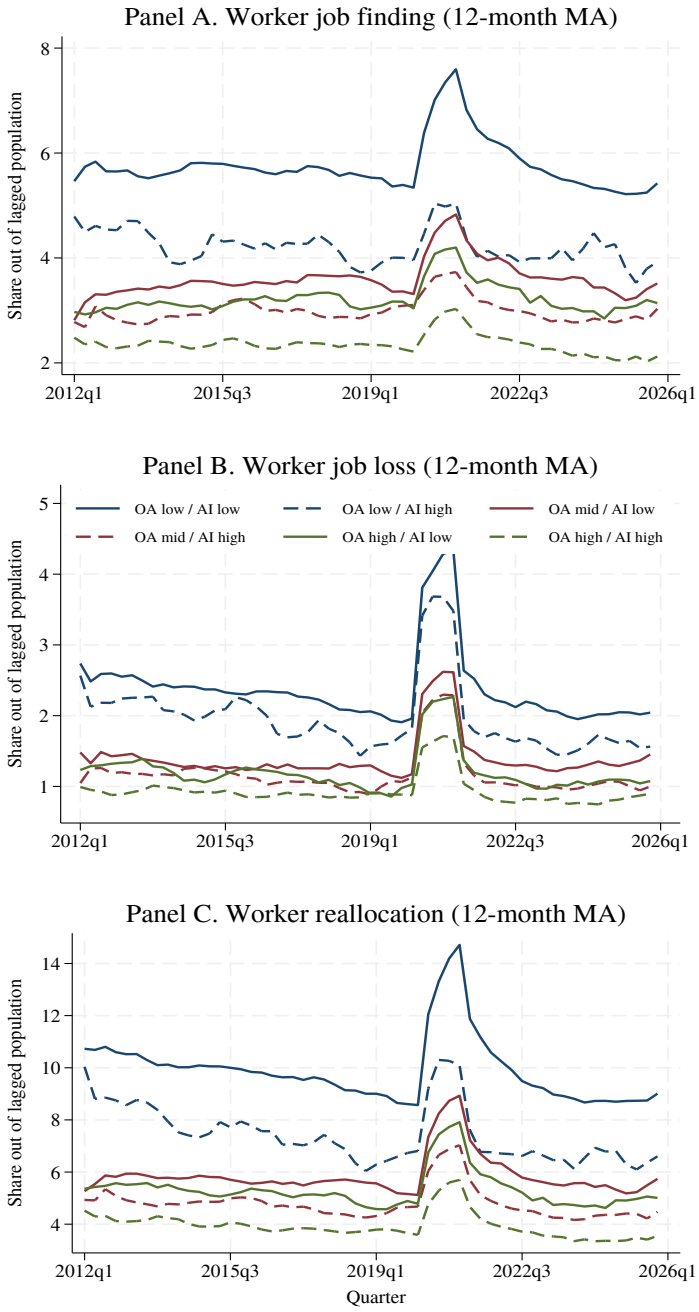
We compute market tightness for four groups of workers defined by AI exposure and AI adoption. Figure 8 presents market tightness across these groups—distinguishing workers whose AI exposure is above or below the mean and whose industry-level AI adoption is above or below the median. Panel A reports estimates based on OpenAI's AI exposure measure, while Panel B uses Anthropic's measure.

Overall, workers with high AI exposure exhibit higher market tightness, consistent with their lower unemployment rates and lower EU transition rates. In addition, workers in occupations with higher AI adoption tend to experience higher market tightness.

However, a notable divergence emerges over time. Market tightness for high-exposure workers—particularly those with both high exposure and high adoption—has remained below its pre-COVID level since 2023, while market tightness for low-exposure workers has largely returned to around its pre-COVID level. that the evolution of tightness across groups cannot be fully explained by aggregate cyclical conditions.

Instead, the market tightness among high-exposure workers points to structural forces associated with AI adoption. While these workers continue to experience relatively favorable labor market conditions in cross section, the persistent shortfall relative to pre-COVID levels indicates weaker vacancy creation in high-exposure occupations. This is consistent with firms

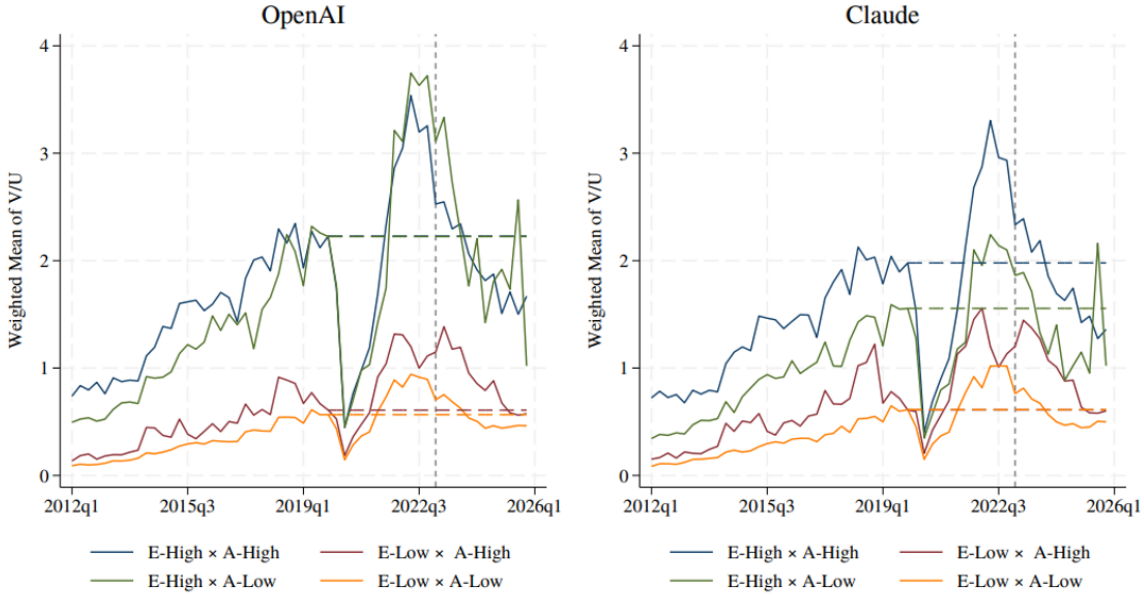
Figure 7: WORKER FLOWS BY AI EXPOSURE AND ADOPTION



Note: This figure plots the fractions of job creation and job destruction relative to payroll employment by AI exposure and adoption in Panels A and B, respectively. Panel C displays the total reallocation rate, defined as the sum of job creation and destruction, by AI exposure and adoption.

Source: Authors' calculation.

Figure 8: MARKET TIGHTNESS BY AI-EXPOSURE AND ADOPTION



Note: E-High (E-Low) denotes high (low) AI exposure, and A-High (A-Low) denotes high (low) AI adoption.
Source: Authors' calculation.

adjusting labor demand through task reorganization and partial substitution of labor with AI technologies.

6 Dispersions in job losses and job findings and AI-driven reallocation pressure

This section reports the variance decomposition result described in Section 2.3. The cross-sectional variance of job-finding rates among the unemployed admits the decomposition:

$$D_t^{(f)} \equiv \mathrm{Var}_t\left(f_{it}\right) = \underbrace{\mathrm{Var}_j\left(E_a\left[f_{it} \mid j,a\right]\right)}_{\text{between-industry component}} + \underbrace{E_j\left[\mathrm{Var}_a\left(E_t\left[f_{it} \mid j,a\right] \mid j\right)\right]}_{\text{within-industry, between-AI component}} + \underbrace{E_{j,a}\left[\mathrm{Var}_t\left(f_{it} \mid j,a\right)\right]}_{\text{within-industry, within-AI component}},$$

where j denotes industry and a denotes AI exposure-adoption. We use detailed 1990 industry classifications (`ind1990` in IPUMS) and define deciles of AI exposure and those of AI adoption.

The above decomposition can be applied to the job-loss rates.

Figure 9 reports the total cross-sectional variance in job-finding rates, along with the portions attributable to differences across industries (between-industry component), differences in AI exposure (between-AI component), and the residual (within-AI component).

The overall dispersion (solid blue line in the upper panel) rises steadily through 2020 and remains elevated through the end of 2025. Given that the aggregate job-finding rate was improving after the Great Recession until the onset of the COVID-19 pandemic, the increase in dispersion points to growing reallocation frictions or mismatch within the unemployment pool.

Importantly, the rise in dispersion is driven by both industry and AI-related factors, with the latter playing a larger role. The AI component accounts for roughly 40% of the total dispersion (green dashed line in the bottom panel), whereas industry heterogeneity explains a smaller share. This result suggests that heterogeneity in AI exposure and adoption is an important factor for the reallocation pressure and the disparities in job findings, and further implies its importance in structural unemployment.[6]

Meanwhile, both AI factors and industry play a limited role in the dispersion of separation rates (Figure 10). As shown in the upper panel, the total dispersion is largely driven by the within-industry, within-AI component (the residual). Although AI factors remain more important than industry heterogeneity in explaining separation dispersion, both components account for less than 20% of the total variation in separation rates.

All told, AI factors are an important driver of the increase in dispersion in job-finding rates after the Great Recession and their persistently elevated levels following the COVID-19 pandemic, whereas their role in disparities in separation rates appears more limited. AI raises reallocation pressure and mismatch primarily through the hiring margin rather than the separation margin.

[6] Considering a more aggregated classification with 13 industries, the increase in dispersion is entirely accounted for by AI-related factors. This observation suggests that AI exposure and adoption are closely associated with industry characteristics. We further consider the decomposition for each broader industry, and the results are in the appendix.

Figure 9: DECOMPOSITION OF JOB-FINDING DISPERSION

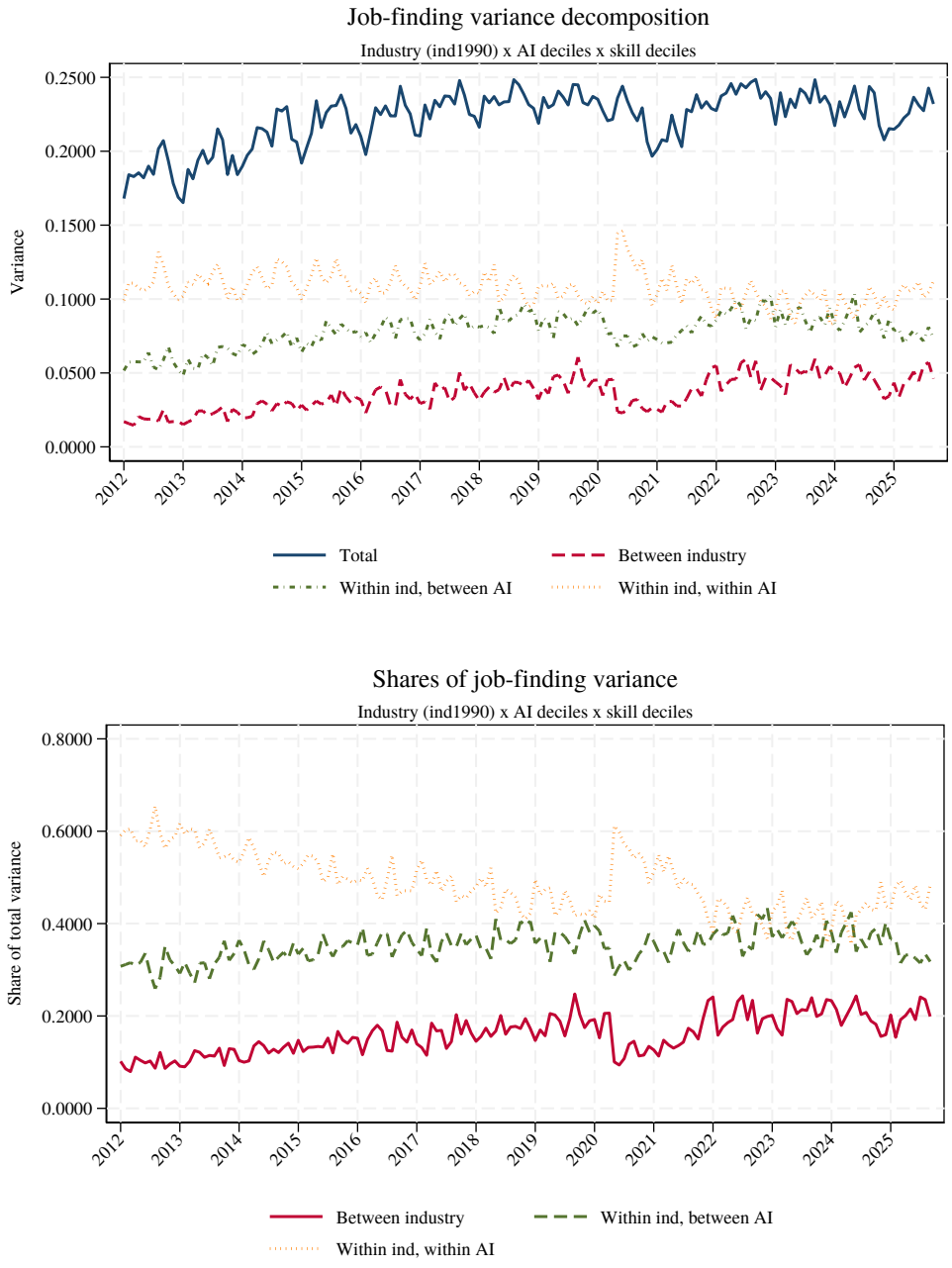
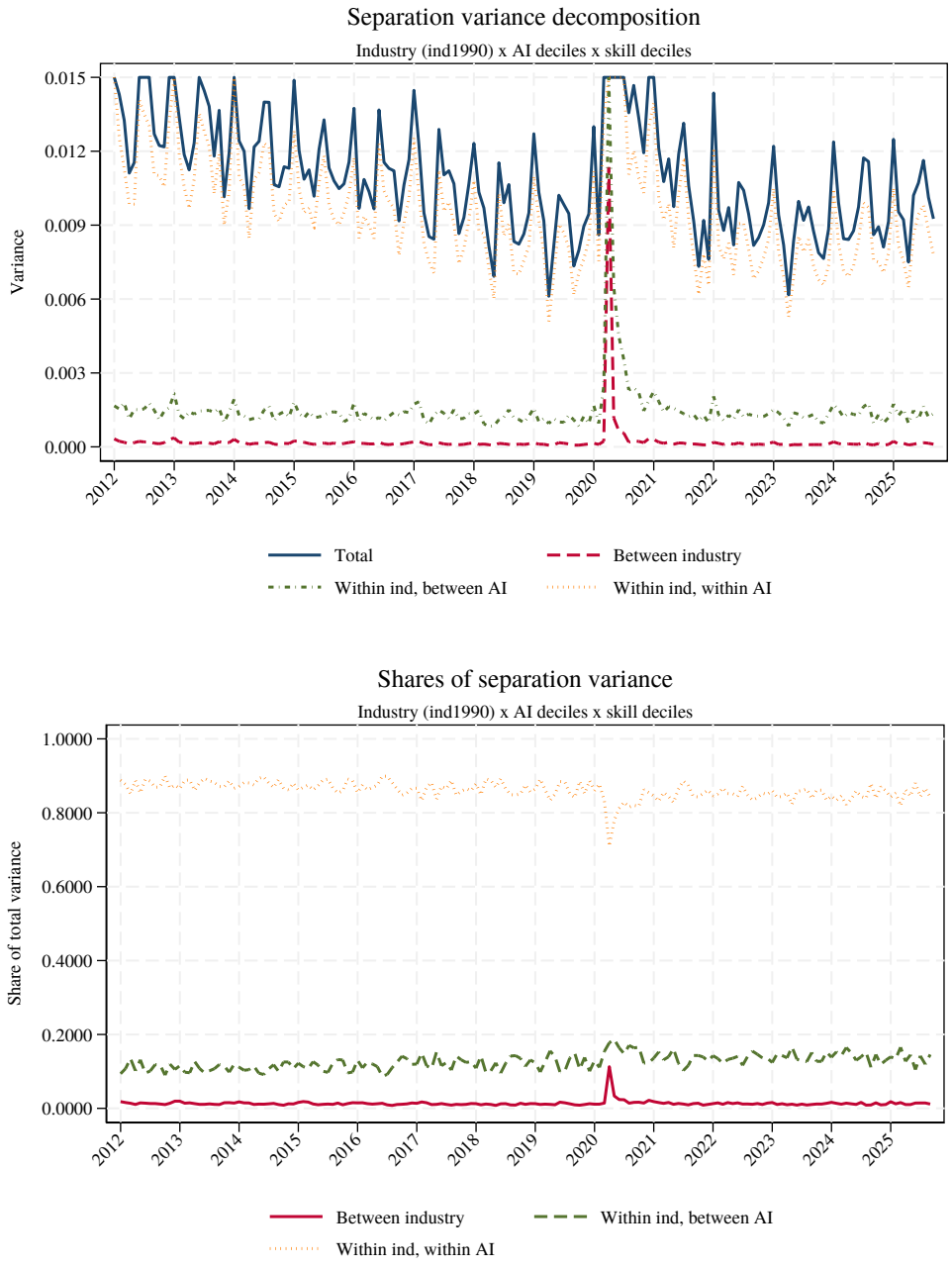


Figure 10: DECOMPOSITION OF SEPARATION DISPERSION



7 Indices of hirability and separability and the latent reallocation pressure

This section formally analyzes the effects of AI exposure and adoption on job finding and job loss. While the cross-sectional variance decomposition provides insights into the roles of AI and industry in shaping the dispersion of these rates, it may be sensitive to the inclusion of additional factors. Moreover, dispersion alone may not fully capture changes in the tails of the distribution, which are not well summarized by the second moment.

To address these issues, we estimate individual-level regressions of job-finding incidences on AI exposure and AI adoption, controlling for a range of worker-level characteristics. Using these estimates, we construct an individual-level hirability index and explore its implications for AI-attributable disparities in labor market outcomes. Since transitions from unemployment to employment are not observed for all individuals in the CPS, we impute hirability for those who lose their jobs and remain unemployed. We then measure the dispersion of the hirability index to capture reallocation pressure and assess the extent to which AI has contributed to it. We apply the same approach to transitions from employment to unemployment and from nonparticipation to employment.

7.1 Model for the hirability index

The baseline pooled regression is

$$UE_{it} = \alpha + \beta_1 mis_{it} + \beta_2 AIX_{it} + \beta_3 AIA_{it} + \beta_4 \theta_{i,t-1} + \beta_5 age_{it} + \beta_6 age_{it}^2 + \beta_7 sex_i + \beta_8 edu_i + \varepsilon_{it},$$

where UE_{it} is the indicator of E-to-U transitions between $t-1$ and t, mis_{it} is the month-in-sample indicator, AIX_{it} is the AI exposure, AIA_{it} is the AI adoption rate, $\theta_{i,t-1}$ is the market tightness (V/U) of the individaul's industry in the previous period, age_{it} and age_{it}^2 are age and the squared age, sex_{it} is the gender, edu_{it} is the education categories – less than high school, high-school graduation, some college and associate degree, and college graduation, and ε_{it} is the residual. We consider mis_{it} to control potential rotation group bias in the reported employment

and unnemployment status (Ahn and Hamilton, 2022). The standard errors are clustered at the individual level. As the baseline specification, we restrict our sample period from 2023 onward, because the observations of AI adoption in the job postings are large enough during this period.

Note that industry-level heterogeneity and supply-demand conditions are captured by θ_{it}. In addition, since AI exposure varies at the occupation level, the model also accounts for an individual's occupation as well.

After we estimate the model, we recover the fitted value $\widehat{UE}_{it}$ based on the estimated coefficients for all i and t. We call $\hat{UE}_{it}$ *"the hirability index."*

To remove the contribution of AI exposure and AI adoption, we construct an "AI-purged" fitted value. Since the regression includes both $openAI3m_{it}$ and ai_skill_{it}, we define

$$\widehat{UE}_{it}^{wo} = \widehat{UE}_{it} - \widehat{\beta_2}\, AIX_{it} - \widehat{\beta_3}\, AIA_{it}. \tag{7.1}$$

7.2 Cross-sectional dispersion over time

We then measure the dispersion of the hirability index across individuals over time to capture the reallocation pressure that individuals face. Higher dispersion implies that a larger subset of individuals would have difficulty finding a job when unemployed.

First, we estimate the cross-sectional mean of the individual-level hirability index as follows:

$$\mu_t^w = \frac{\sum_i w_{it} \widehat{UE}_{it}}{\sum_i w_{it}}. \tag{7.2}$$

The weighted cross-sectional standard deviation is

$$sd_t^w = \sqrt{\frac{\sum_i w_{it} \left(\widehat{UE}_{it} - \mu_t^w\right)^2}{\sum_i w_{it}}}. \tag{7.3}$$

Analogously, for the AI-purged fitted values $\widehat{UE}_{it}^{wo}$, the weighted mean and standard deviation are

$$\mu_{t,wo}^w = \frac{\sum_i w_{it} \widehat{UE}_{it}^{wo}}{\sum_i w_{it}}, \tag{7.4}$$

and

$$sd^{w}_{t,wo} = \sqrt{\frac{\sum_i w_{it}\left(\widehat{UE}^{wo}_{it} - \mu^{w}_{t,wo}\right)^2}{\sum_i w_{it}}}. \tag{7.5}$$

7.3 Hirability index and its dispersion over time

Table 3 reports the regression results. Columns A and B present the estimated coefficients for the full sample period and for the period beginning in 2023, respectively. Since the hirability index is constructed using the latter set of coefficients, we focus our discussion on Column B.

Overall, these results highlight that AI-related factors have become increasingly important determinants of job finding. A key finding is that AI exposure is strongly associated with a lower probability of job loss: the coefficient on openAI3m is negative and highly statistically significant in both specifications, with a somewhat larger magnitude in the post-2022 sample. This pattern suggests that workers in more AI-exposed occupations experience reduced job finding, consistent with negative AI effects on the hiring margin [Hosseini and Lichtinger, 2025].

In addition, AI adoption—the share of postings requiring AI-related skill—exhibits a similar but more heterogeneous pattern. While the coefficient is negative but imprecisely estimated in the full sample, it becomes large, negative, and statistically significant in the post-2023 period, indicating that AI adoption at the industry level is increasingly associated with lower job finding. In contrast, labor market tightness (θ_{t-1}) does not have a statistically significant effect, suggesting that cyclical conditions play a more limited role in explaining cross-sectional variation in separability relative to structural factors such as AI exposure.

Hirability declines with age at a decreasing rate, as indicated by the negative coefficient on age and positive coefficient on age squared. Female workers exhibit a higher likelihood of job finding, particularly in the post-2023 period. Educational gradients also shift over time: while higher education is associated with higher job finding in the full sample, the relationship reverses for college-educated workers in the post-2023 period, potentially reflecting that AI has negative effects on highly educated workers unlike the pre-LLM period.[7]

In Figure 11, Panel A shows the mean hirability index by quartile of AI exposure. The mean

[7] The statistically significant coefficients on month-in-sample indicators reflect rotation patterns in transitions from unemployment to employment.

hirability index is lower for individuals with higher AI exposure. Moreover, the mean hirability index of the highest AI exposure quartile has declined since 2022 and fallen more sharply in 2024 and 2025, while those of the other quartiles remain roughly flat.

Panel B of Figure 11 shows the mean hirability index by quartile of AI adoption. The mean hirability index is lower for individuals with higher exposure to AI adoption. Recent increases in AI adoption have lowered the hirability of those with less AI adoption exposure, while slightly raising that of those with more. Therefore, unlike AI exposure, AI adoption does not show signs of increased dispersion in hirability.

Figure 12 displays the standard deviation of the hirability index. The dispersion remained largely flat before 2023, then increased steadily and picked up more rapidly from 2024 onward, suggesting that reallocation pressure has risen significantly following the introduction of large language models. By contrast, the dispersion of the hirability index purged of AI factors remains flat throughout. This result highlights that AI is the main driver of the increased dispersion in hirability and the primary source of heightened reallocation pressure.

Table 3: DETERMINANTS OF HIRABILITY

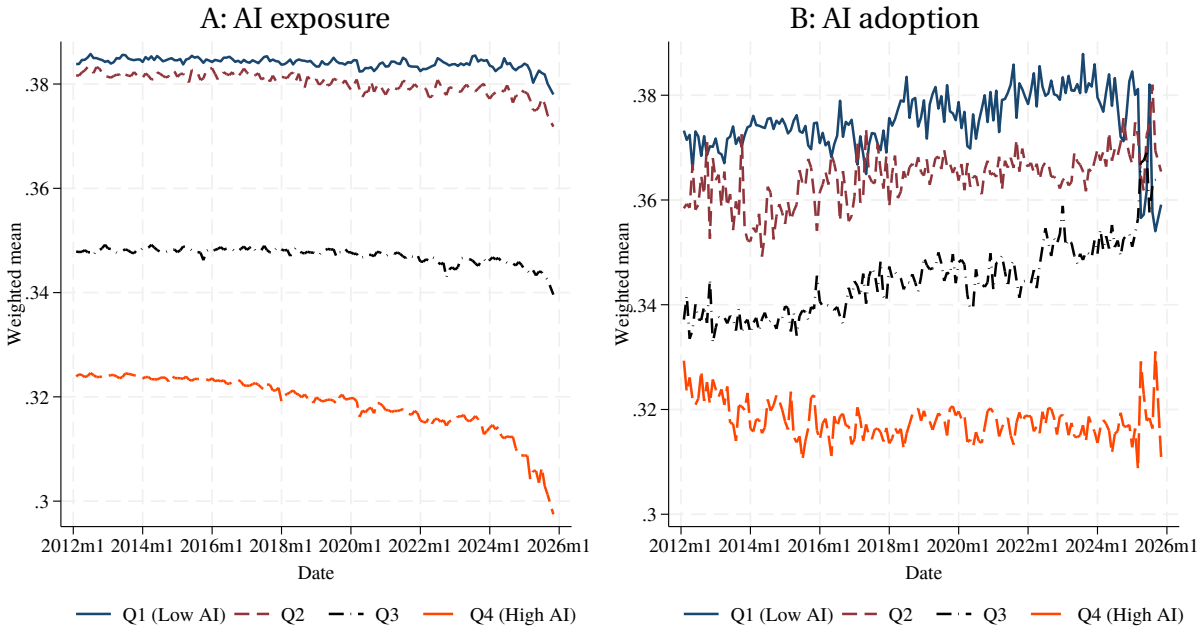
	(1) All sample	(2) 2023 on
openAI3m	-0.110***	-0.116***
	(0.00575)	(0.0178)
Share of postings with an AI skill	-0.101	-0.429***
	(0.0821)	(0.118)
theta_lag	-0.0000119	-0.000108
	(0.0000746)	(0.000121)
age	-0.00924***	-0.00559***
	(0.000408)	(0.00113)
age2	0.0000886***	0.0000529***
	(0.00000473)	(0.0000129)
female	0.0149***	0.0393***
	(0.00217)	(0.00636)
HS grad	-0.00977***	-0.0285***
	(0.00341)	(0.0105)
Some college / AA	0.0137***	0.00244
	(0.00361)	(0.0113)
College+	0.0292***	-0.0287**
	(0.00396)	(0.0118)
Observations	233221	27816
R-squared	0.00848	0.0111

Standard errors in parentheses

Standard errors clustered at the individual level. Constant and coefficients on MIS are not reported.

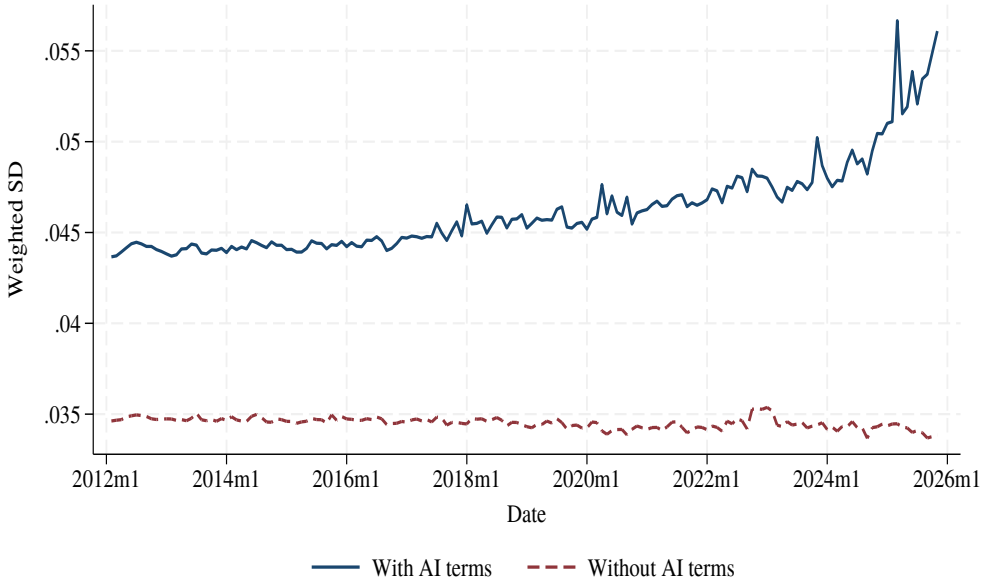
* $p < 0.10$, ** $p < 0.05$, *** $p < 0.01$

Figure 11: HIRABILITY INDEX BY THE QUARTILE OF AI EXPOSURE AND AI ADOPTION



Note: Panel A displays the mean hirability index by the quartile of AI exposure. Panel B displays the mean hirability index by the quartile of AI adoption.
Source: Authors' calculation.

Figure 12: DISPERSION OF HIRABILITY INDEX WITH AND WITHOUT AI FACTORS



Note: This figure plots the dispersion of hirability index with AI exposure and adoption (solid blue line) and that without AI exposure and adoption (dashed red line).
Source: Authors' calculation.

7.4 Separability Index and the dispersion of E-to-U transitions

Next, we examine the extent to which AI has affected job separations, as measured by transitions from employment to unemployment (E→U). To this end, we apply the same empirical framework to model the individual likelihood of job separation. Specifically, we replace the dependent variable in (7.1) with EU_{it} and compute the fitted values $\widehat{EU}_{it}$ for all individuals i and periods t based on the estimated coefficients. We refer to $\widehat{EU}_{it}$ as the *"separation index."* Using this index, we construct measures of cross-sectional dispersion both with and without the AI-related factors.

Table 4 reports estimates of the determinants of the separation index, measured by transitions from employment to unemployment. Column (1) presents results for the full sample, while column (2) restricts the sample to the post-2022 period. Across both specifications, AI exposure is associated with a statistically significant decline in the likelihood of job separation. The magnitude of the coefficient is somewhat smaller in the post-2022 sample, but remains economically modest and precisely estimated, indicating that workers in more AI-exposed environments are less likely to transition from employment to unemployment.

In contrast, AI adoption, measured by the share of postings requiring AI-related skills, is positively associated with job separations, and the effect becomes larger in the post-2022 sample. This pattern suggests that while exposure to AI may be associated with greater job stability, the adoption of AI technologies is linked to increased reallocation pressures, particularly in the recent period following the diffusion of LLMs.

Labor market tightness is negatively related to separations in both samples, consistent with standard search-and-matching models. Notably, the magnitude of this effect declines in the post-2022 sample, suggesting that the stabilizing role of tight labor markets in reducing separations may have weakened somewhat in the recent period.

The demographic controls exhibit patterns consistent with life-cycle dynamics. The probability of separation declines with age at a decreasing rate, as indicated by the negative coefficient on age and the positive coefficient on age squared. Gender differences are small and statistically insignificant. Educational attainment is strongly associated with lower separation risk: relative to individuals with less than a high school education, all higher education groups experience signif-

icantly lower separation probabilities, with the largest reductions observed for college-educated workers.

Overall, the comparison between the two sample periods indicates that the qualitative relationships are robust across samples, but the post-2022 period is characterized by a stronger association between AI adoption and job separations. This provides suggestive evidence that recent advances in AI, particularly the diffusion of LLMs, may have intensified reallocation dynamics through the separation margin, even as exposure to AI remains associated with lower separation risk.

Figure 13 plots the separability index by quartiles of AI exposure and AI adoption. In contrast to the hirability index, the separation index by AI exposure does not exhibit any notable change following the introduction of LLMs. However, beginning in 2025, the separability index increases for workers in high–AI-adoption occupations, while it declines for those in low–AI-adoption occupations.

Figure 14 plots the dispersion of the separation index. Relative to the dispersion of the hirability index, the dispersion of the separation index shows no noticeable change after 2024:Q4 and remains broadly similar to that of the separation index constructed without AI-related factors. These results suggest that AI-driven reallocation pressures operate primarily through the hiring margin rather than through separations, at least through late 2025.

Table 4: DETERMINANTS OF SEPARABILITY INDEX

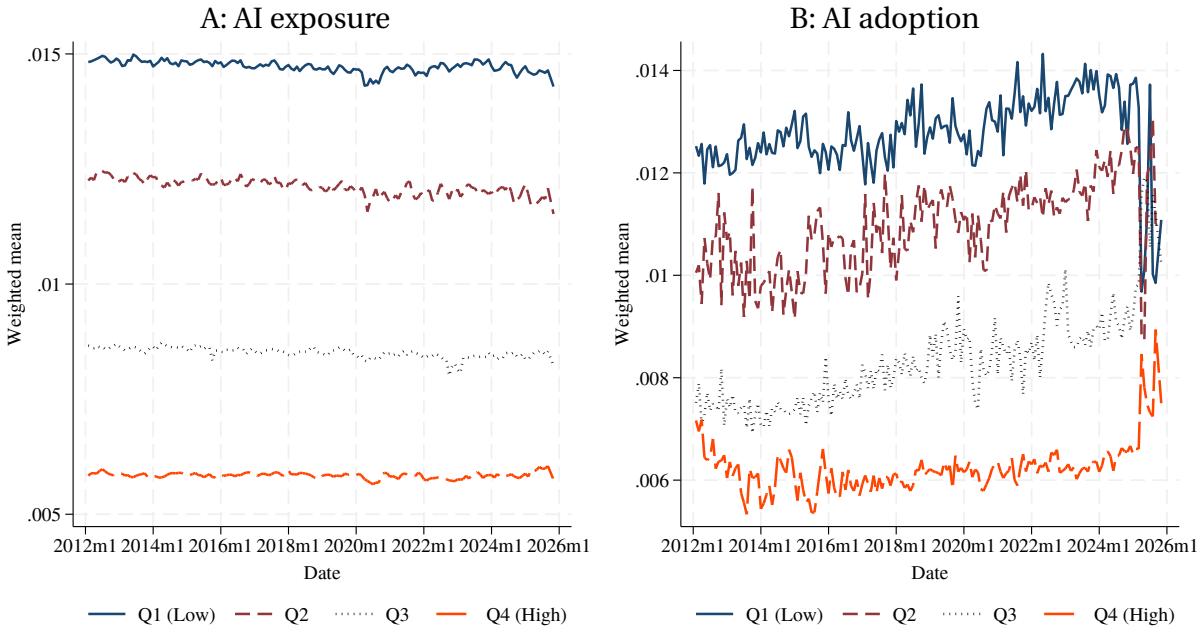
	(1)	(2)
	All sample	2023 on
openAI3m	-0.0154***	-0.0114***
	(0.000248)	(0.000553)
Share of postings with an AI skill	0.00655***	0.00980***
	(0.00207)	(0.00269)
theta_lag	-0.0000257***	-0.0000159***
	(0.00000127)	(0.00000174)
age	-0.000947***	-0.000782***
	(0.0000208)	(0.0000448)
age2	0.00000870***	0.00000703***
	(0.000000221)	(0.000000470)
female	-0.0000588	-0.0000477
	(0.0000892)	(0.000195)
HS grad	-0.00583***	-0.00508***
	(0.000258)	(0.000593)
Some college / AA	-0.00784***	-0.00700***
	(0.000254)	(0.000586)
College+	-0.0106***	-0.00886***
	(0.000248)	(0.000572)
Observations	6135368	1019222
R-squared	0.00379	0.00308

Standard errors in parentheses

Standard errors clustered at the individual level. Constant and coefficients on MIS are not reported.

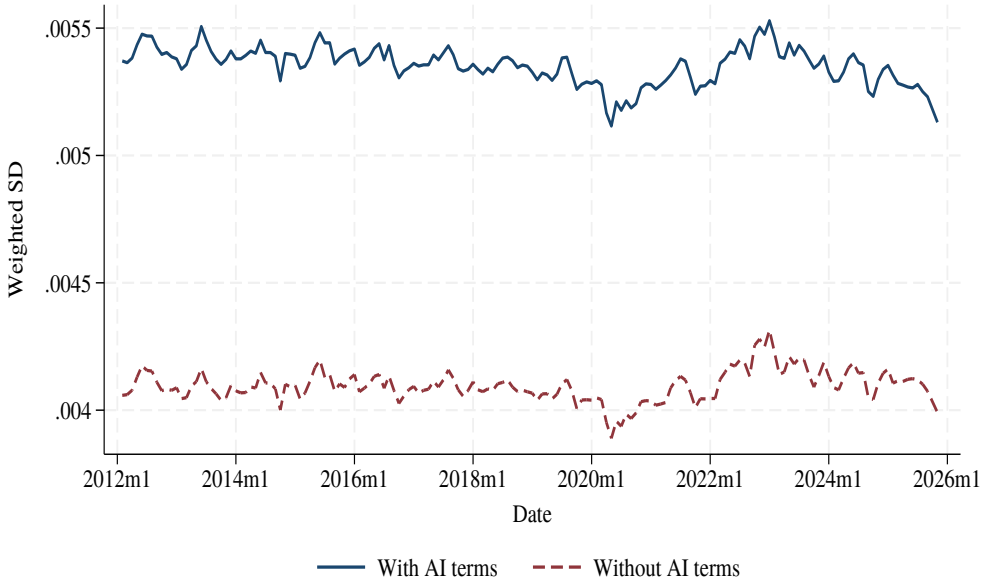
* $p < 0.10$, ** $p < 0.05$, *** $p < 0.01$

Figure 13: SEPARABILITY INDEX BY THE QUARTILE OF AI EXPOSURE AND AI ADOPTION



Note: Panel A displays the mean separability index by the quartile of AI exposure. Panel B displays the mean separability index by the quartile of AI adoption.
Source: Authors' calculation.

Figure 14: DISPERSION OF SEPARABILITY INDEX WITH AND WITHOUT AI FACTORS



Note: This figure plots the dispersion of hirability index with AI exposure and adoption (solid blue line) and that without AI exposure and adoption (dashed red line).
Source: Authors' calculation.

8 Implications for wages, hours worked, and the U-star

Section 8.1 discusses the effects of AI and AI-driven reallocation on wage and labor productivity growth, while Section 8.2 examines the implications for the natural rate of unemployment.

8.1 Effects of AI on wage and productivity growths

Consider a regression model for the wage growth:

$$\begin{aligned} w_{it} = {} & \beta_1 \, openAI_{it} + \beta_2 \left(openAI_{it} \times llm_dum_t \right) \\ & + \beta_3 \, ai_skill_{it} + \beta_4 \left(ai_skill_{it} \times llm_dum_t \right) \\ & + \beta_5 \theta_{it} + \beta_6 \, age_{it} + \beta_7 \, age_{it}^2 \\ & + \gamma' X_{it} + \delta_t + \eta_{j(i)} + \varepsilon_{it}, \end{aligned}$$

where w_{it} is the 12-month nominal hourly wage growth of individual i at time t, $openAI_{it}$ denotes the individual's AI exposure, ai_skill_{it} captures AI adoption at the individual's industry, llm_dum_t is a dummy variable equal to one for 2023 onward, θ_{it} denotes market tightness, age_{it} and age_{it}^2 are the individual's age and its square, X_{it} includes gender and education controls, δ_t represents time fixed effects, and $\eta_{j(i)}$ denotes industry fixed effects.

Table 5 reports the regression results. AI-related factors are important determinants of wage inflation: Column (1) reports the result without industry fixed effects (`ind1990`) and column (2) reports the result with industry fixed effects. Both AI exposure and AI skill share are positively and statistically significantly associated with wage inflation, suggesting that workers in more AI-exposed occupations and industries with higher AI adoption experience faster wage growth. However, the interaction terms with the LLM period are negative and statistically significant, implying that these positive effects are attenuated after the introduction of LLMs. Quantitatively, the coefficients indicate a substantial reduction in the marginal impact of both AI exposure and AI skill share on wage inflation in the post-LLM period. This pattern is consistent with the interpretation that while AI initially complements high-exposure workers and boosts their wages, the diffusion of LLM technologies may compress wage growth by facilitating task substitution or

reducing hirings for these workers. The inclusion of time fixed effects, industry fixed effects, and industry-level market tightness suggest that the negative effects of LLM's are unlikely to reflect cyclical weakness in labor demand.

We replace the wage growth with hours worked to assess AI's effects on hours worked. Table 6 reports the regression results of hours worked. Overall, AI exposure is positively and significantly associated with hours worked, indicating that workers in more AI-exposed occupations tend to supply more labor and work longer hours. However, the interaction with the LLM period (2023 onward) is negative and highly significant, suggesting that this positive relationship weakens following the introduction of LLM technologies. In contrast, AI adoption—as captured by the AI skill share—has a negative baseline effect on hours worked, consistent with automation reducing labor input. Importantly, the interaction with the LLM period is positive and statistically significant, indicating that this negative effect is attenuated, and partially reversed, in the post-LLM period. These findings suggest a shift in the role of AI from labor-substituting to more labor-complementary along the adoption margin, while the labor-supply effect associated with AI exposure diminishes over time. The similarity of these patterns in the post-2023 sample reinforces the interpretation that LLM technologies have materially altered how AI exposure and adoption translate into labor input decisions.

Table 5: DETERMINANTS OF WAGE INFLATION

	(1) WO industry FE	(2) W/ industry FE
AI exposure	3.197***	2.993***
	(0.402)	(0.434)
AI exposure × LLM period	-1.581*	-1.615*
	(0.880)	(0.880)
AI skill share	56.36***	41.85***
	(14.31)	(13.58)
AI skill share × LLM period	-36.01**	-26.04*
	(16.48)	(15.75)
Market tightness	0.0176***	0.0154***
	(0.00575)	(0.00577)
Age	-0.223***	-0.369***
	(0.0274)	(0.0288)
Age squared	0.00135***	0.00279***
	(0.000311)	(0.000324)
Female	-1.662***	-1.077***
	(0.150)	(0.170)
High-school graduation	1.622***	1.292***
	(0.239)	(0.242)
Some college and associate degree	1.294***	0.868***
	(0.242)	(0.249)
College graduation	2.289***	1.769***
	(0.289)	(0.299)
Observations	293641	293641
R-squared	0.00454	0.00686

Standard errors in parentheses

Time fixed effects are included in both columns.

* $p < 0.10$, ** $p < 0.05$, *** $p < 0.01$

Table 6: DETERMINANTS OF HOURS WORKED

	(1) WO industry FE	(2) W/ industry FE
AI exposure	3.850***	3.237***
	(0.0758)	(0.0826)
AI exposure × LLM period	-0.606***	-0.584***
	(0.175)	(0.173)
AI skill share	-8.403***	-8.637***
	(0.948)	(0.964)
AI skill share × LLM period	4.607***	4.835***
	(1.330)	(1.328)
Market tightness	0.00704***	0.00495***
	(0.000627)	(0.000622)
Age	1.145***	1.046***
	(0.00651)	(0.00651)
Age squared	-0.0125***	-0.0115***
	(0.0000725)	(0.0000723)
Female	-4.800***	-3.898***
	(0.0270)	(0.0302)
High-school graduation	2.581***	2.332***
	(0.0609)	(0.0603)
Some college and associate degree	2.281***	2.161***
	(0.0621)	(0.0621)
College graduation	3.286***	3.472***
	(0.0622)	(0.0636)
Observations	777636	777635
R-squared	0.0977	0.121

Standard errors in parentheses

Time fixed effects are included in both columns.

* $p < 0.10$, ** $p < 0.05$, *** $p < 0.01$

8.2 Implications for the natural rate of unemployment

To assess the effects of LLMs on the NRU, we estimate group-specific NRUs for high- and low-AI-exposure workers using the trend components of their unemployment inflow and outflow rates, and then aggregate these estimates using their respective labor force shares. Specifically, we extract trend components of unemployment flows rates using a Bayesian trend–cycle decomposition and feed them into Shimer [2012]'s steady-state unemployment framework, which is adopted by Tasci [2012], Crump et al. [2019], Ahn [2023].

Because our AI exposure measures are available only from 2011 onward, the trend–cycle decomposition is subject to additional uncertainty. Accordingly, we interpret this empirical exercise as providing directional evidence on the risks to natural rate estimates that abstract from AI-driven reallocation effects.

Trend–cycle decomposition by AI exposure. Let $g \in \{H, L\}$ index AI-exposed and AI-nonexposed workers. We decompose the unemployment inflow and outflow rates into trend and cyclical components:

$$s_{gt} = \tau^s_{gt} + c^s_{gt} + r^s_{gt} \qquad r^s_{gt} \sim N(0, R_s) \tag{8.1}$$

$$f_{gt} = \tau^f_{gt} + c^f_{gt} + r^f_{gt} \qquad r^f_{gt} \sim N(0, R_f), \tag{8.2}$$

where r^s_{gt} and r^f_{gt} are the measuremenmt errors that are assumed to be normal and mean zero.

In our application, the trend in the inflow rate is specified as a local level, while the trend in the outflow rate is specified as a local linear trend. The cyclical components may be modeled as stationary autoregressive processes. More concretely, a stochastic version of the model is given by

$$\tau^s_{gt} = \tau^s_{g,t-1} + \nu^s_{gt}, \tag{8.3}$$

$$\tau^f_{gt} = \tau^f_{g,t-1} + \beta^f_{g,t-1} + \nu^f_{gt}, \tag{8.4}$$

$$\beta^f_{gt} = \beta^f_{g,t-1} + \kappa^f_{gt}, \tag{8.5}$$

$$c^s_{gt} = \phi^s_g c^s_{g,t-1} + \omega^s_{gt}, \tag{8.6}$$

$$c^f_{gt} = \phi^f_g c^f_{g,t-1} + \omega^f_{gt}, \tag{8.7}$$

with Gaussian shocks

$$\nu^s_{gt} \sim \mathcal{N}(0, \sigma^2_{\nu^s,g}), \quad \nu^f_{gt} \sim \mathcal{N}(0, \sigma^2_{\nu^f,g}), \quad \kappa^f_{gt} \sim \mathcal{N}(0, \sigma^2_{\kappa^f,g}),$$

and similarly for the cyclical shocks. This system is estimated with a Bayesian method, and the details are found in the appendix.

Group-specific natural rate. Given the trend components of inflow and outflow rates, the group-specific natural rate of unemployment is defined as

$$u^*_{gt} = \frac{\tau^s_{gt}}{\tau^s_{gt} + \tau^f_{gt}}. \tag{8.8}$$

Aggregate natural rate. The aggregate natural rate is obtained as the labor-force-share-weighted average of group-specific natural rates:

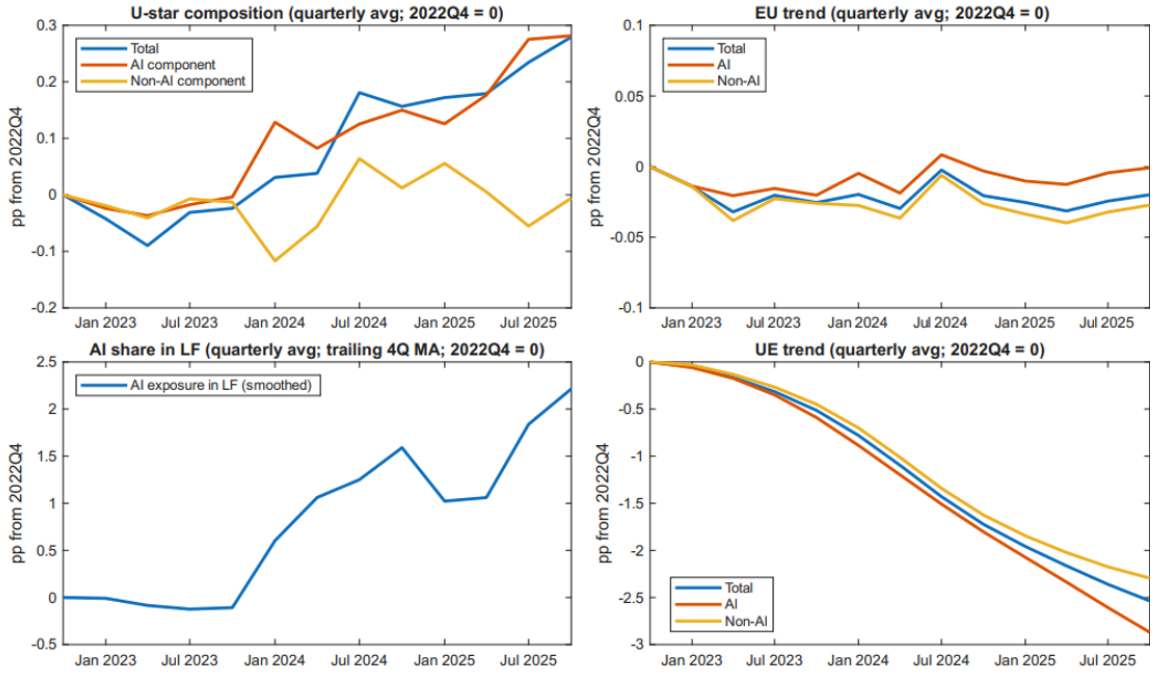
$$u^*_t = \sum_{g \in \{H,L\}} \omega_{gt}\, u^*_{gt}, \qquad \sum_{g \in \{H,L\}} \omega_{gt} = 1, \tag{8.9}$$

where ω_{gt} denotes the labor force share of group g at time t. Details about the estimation are in the appendix.

Figure 15 displays changes in the natural rate of unemployment driven by high- and low-exposure groups (top left), share of high AI-exposed workers (bottom left), the trend separation rate (top right), and the trend job-finding rate (bottom right).

The modestly faster decline in the trend job-finding rate among high-exposure workers, together with their rising labor force share, has raised the NRU, while trend job-loss rates have remained broadly stable. Consistently, market tightness for high-exposure workers has remained below the pre-COVID level since 2023, while that for low-exposure workers is around the pre-COVID level.

Figure 15: NATURAL RATE OF UNEMPLOYMENT BY AI EXPOSURE



Note to figure: This figure displays changes in the natural rate of unemployment driven by high- and low- exposure groups (top left), share of high AI-exposed workers (bottom left), the trend separation rate (top right), and the trend job-finding rate (bottom righ). Total is shown in blue, high exposure in red, and low exposure in yellow.

Note to figure: Authors; calculation.

9 Conclusion

This paper studies how artificial intelligence shapes labor market dynamics through its effects on worker flows, reallocation, and equilibrium unemployment. Combining worker-level AI exposure with CPS micro data and measures of AI adoption, we document systematic differences in labor market outcomes across exposure groups and over time, particularly following the diffusion of large language models (LLMs).

We show that workers with higher AI exposure exhibit lower unemployment rates, driven primarily by lower separation rates and stronger labor force attachment. At the same time, recent developments in AI are associated with a decline in job-finding rates among highly exposed workers relative to others, alongside reduced job-to-job transitions and increased within-job activity switching. These patterns suggest that adjustment to AI operates increasingly through task reorganization within firms rather than worker reallocation across employers.

Consistent with this interpretation, we document a rise in dispersion in job-finding prospects since 2023, driven by AI exposure and adoption. Through the lens of standard search-and-matching frameworks, this increase in dispersion signals elevated reallocation pressures and a higher degree of mismatch in the labor market. We further find that the positive association between AI and wage growth and hours worked in the pre-LLM period has weakened, pointing to a softening of labor demand for highly exposed workers.

Finally, using a Bayesian trend–cycle decomposition of unemployment flows by AI exposure, we estimate that the natural rate of unemployment has increased modestly—by about a quarter percentage point—since 2022:Q4, although this estimate remains subject to considerable uncertainty.

Overall, our findings suggest that the recent wave of AI technologies is reshaping the structure of the labor market by altering reallocation patterns and increasing dispersion in job-finding outcomes, with potential implications for structural unemployment. An important direction for future research is to develop structural models that can jointly account for task-level technological change, firm adjustment, and worker heterogeneity in order to better quantify the long-run effects of AI on labor markets.

References

Katharine G. Abraham and Lawrence F. Katz. Cyclical unemployment: Sectoral shifts or aggregate disturbances? *Journal of Political Economy*, 94(3):507–522, 1986. ISSN 00223808, 1537534X. URL http://www.jstor.org/stable/1833046.

Daron Acemoglu. The simple macroeconomics of ai. *Economic Policy*, 40(121):13–58, 2025.

Daron Acemoglu, David Autor, Jonathon Hazell, and Pascual Restrepo. Artificial intelligence and jobs: Evidence from online vacancies. *Journal of Labor Economics*, 40(S1):293–340, 2022.

Hie Joo Ahn. Duration structure of unemployment hazards and the trend unemployment rate. *Journal of Economic Dynamics and Control*, 151:104670, 2023. ISSN 0165-1889. doi: 10.1016/j.jedc.2023.104670.

Hie Joo Ahn, Bart Hobijn, and Aysegul Sahin. The Dual U.S. Labor Market Uncovered. Finance and Economics Discussion Series 2023-031, Board of Governors of the Federal Reserve System (U.S.), May 2023. URL https://ideas.repec.org/p/fip/fedgfe/2023-31.html.

Erik Brynjolfsson, Tom Mitchell, and Daniel Rock. What can machines learn, and what does it mean for occupations and the economy? *AEA Papers and Proceedings*, 108:43–47, 2018.

Erik Brynjolfsson, Bharat Chandar, and Ruyu Chen. Canaries in the coal mine?: Six facts about the recent employment effects of artificial intelligence. Working Paper, 2025a.

Erik Brynjolfsson, Danielle Li, and Lindsey Raymond. Generative ai at work*. *The Quarterly Journal of Economics*, 140(2):889–942, 02 2025b. ISSN 0033-5533. doi: 10.1093/qje/qjae044. URL https://doi.org/10.1093/qje/qjae044.

Leland D. Crane and Paul E. Soto. Ai and coder employment: Compiling the evidence. Finance and Economics Discussion Series (FEDS): https://doi.org/10.17016/FEDS.2026.018, 2026.

Richard K. Crump, Stefano Eusepi, Marc Giannoni, and Ayşegül Şahin. A Unified Approach to Measuring u. NBER Working Papers 25930, National Bureau of Economic Research, Inc, June 2019. URL https://ideas.repec.org/p/nbr/nberwo/25930.html.

Z. Cui, M. Demirer, S. Jaffe, L. Musolff, S. Peng, and T. Salz. The effects of generative ai on high skilled work: Evidence from three field experiments with software developers. Available at SSRN 4945566, 2024.

Steven J. Davis, R. Jason Faberman, and John Haltiwanger. Labor market flows in the cross section and over time. *Journal of Monetary Economics*, 59(1):1–18, 2012. ISSN 0304-3932. doi: https://doi.org/10.1016/j.jmoneco.2011.10.001. URL https://www.sciencedirect.com/science/article/pii/S0304393211001000. Carnegie-NYU-Rochester Conference Series on Public Policy at New York University on April 15-16, 2011.

Fabrizio Dell'Acqua, Edward McFowland III, Ethan Mollick, Katherine Kellogg Lifshitz-Assaf, Saran Rajendran, Lisa Krayer, Francois Candelon, and Karim Lakhani. Navigating the jagged

technological frontier: Field experimental evidence of the effects of ai on knowledge worker productivity and quality. Working Paper No. 24-013, Harvard Business School, Cambridge, MA., 2023.

Tyna Eloundou, Sam Manning, Pamela Mishkin, and Daniel Rock. Gpts and gpts: An early look at the labor market impact potential of large language models. arXiv:2303.10130, 2023.

Edward W. Felten, Manav Raj, and Robert Seamans. Occupational heterogeneity in exposure to generative ai. Working Paper, 2023.

Francesco Filippucci, Peter Gal, and Matthias Schief. Aggregate productivity gains from artificial intelligence: A sectoral perspective. Working Paper, 2025.

Menaka Hampole, Dimitris Papanikolaou, Lawrence D.W. Schmidt, and Bryan Seegmiller. Artificial intelligence and the labor market. *NBER Working Paper No. 33509*, 2025.

Kunal Handa, Alex Tamkin, Miles McCain, Saffron Huang, Esin Durmus, Sarah Heck, Jared Mueller, Jerry Hong, Stuart Ritchie, Tim Belonax, Kevin K. Troy, Dario Amodei, Jared Kaplan, Jack Clark, and Deep Ganguli. Which economic tasks are performed with ai? evidence from millions of claude conversations, 2025. URL https://arxiv.org/abs/2503.04761.

Seyed M. Hosseini and Guy Lichtinger. Generative ai as seniority-biased technological change: Evidence from u.s. résumé and job posting data. Working Paper, 2025.

Richard Jackman and Stephen Roper. Structural unemployment. *Oxford Bulletin of Economics and Statistics*, 49(1):9–36, 1987.

David M. Lilien. Sectoral shifts and cyclical unemployment. *Journal of Political Economy*, 90(4): 777–793, 1982. ISSN 00223808, 1537534X. URL http://www.jstor.org/stable/1831352.

Sam J. Manning and TomÃ¡s Aguirre. How adaptable are american workers to ai-induced job displacement? NBER Working Papers 34705, National Bureau of Economic Research, Inc, Jan 2026. URL https://ideas.repec.org/p/nbr/nberwo/34705.html.

George R. Neumann and Robert H. Topel. Employment Risk, Diversification, and Unemployment. *The Quarterly Journal of Economics*, 106(4):1341–1365, 1991. URL https://ideas.repec.org/a/oup/qjecon/v106y1991i4p1341-1365..html.

Shakked Noy and Whitney Zhang. Experimental evidence on the productivity effects of generative artificial intelligence. Available at SSRN 4375283, 2023.

Robert Shimer. Reassessing the ins and outs of unemployment. *Review of Economic Dynamics*, 15(2):127–148, 2012. ISSN 1094-2025. doi: https://doi.org/10.1016/j.red.2012.02.001. URL https://www.sciencedirect.com/science/article/pii/S1094202512000063.

Murat Tasci. The ins and outs of unemployment in the long run: unemployment flows and the natural rate. Working Papers 1224, Federal Reserve Bank of Cleveland, 2012. URL https://ideas.repec.org/p/fip/fedcwp/1224.html.

Kiran Tomlinson, Sonia Jaffe, Will Wang, Scott Counts, and Siddharth Suri. Working with ai: Measuring the occupational implications of generative ai. Working Paper, 2025.

Michael Webb. The impact of artificial intelligence on the labor market. Working Paper, 2020.

Ayşegül Şahin, Joseph Song, Giorgio Topa, and Giovanni L. Violante. Mismatch unemployment. *American Economic Review*, 104(11):3529–3564, November 2014. doi: 10.1257/aer.104.11.3529.

A Appendix

A.1 Job flows

We further examine the effects of AI exposure and adoption on job reallocation. Job reallocation is measured as the sum of job creation and destruction as a percentage of total payroll employment (Davis et al., 2012). We call the fraction of job creation and destruction combined out of payroll employment, as a measure of job reallocation. These measures are available at the industry level, and we merge them with corresponding industry-level measures of AI exposure and adoption.

To assess the effects of AI, we first sort industries into bins based on their AI exposure from OpenAI and AI adoption from Lightcast in each quarter. Industry-level exposure is defined as an employment-weighted average of occupational exposure, while adoption is defined as the fraction of the industry's job postings mentioning an AI-related skill. We form terciles of AI exposure and split AI adoption into high and low groups using the within-quarter median, yielding six groups (e.g., low exposure/low adoption, high exposure/high adoption). We then compute the mean job reallocation measures for each group.

Figure A.1 displays job flows by AI exposure and adoption. In general, both job creation and job destruction are higher in industries with low AI exposure (solid and dashed blue lines), and are particularly elevated in industries with low exposure but high AI adoption (dashed blue line).

Industries with low AI adoption include natural resources and mining, construction, transportation and warehousing, and leisure and hospitality—typically lower-skilled sectors (Table 1). Notably, natural resources and mining exhibits relatively high AI adoption, whereas the others have lower adoption rates. This sector also shows greater churn than others, reflecting seasonal production patterns and employment fluctuations. Such volatility may provide stronger incentives for firms in these industries to adopt AI in order to mitigate production risks and stabilize operations.[8]

[8]This pattern is consistent with the observation that the dispersion in job-finding rates attributable to AI is larger in natural resources and mining industries than high-skilled industries.

Comparing mid- and high-exposure groups, reallocation activity—both job creation and job destruction—is higher in high-exposure industries conditional on high AI adoption. High-exposure, high-adoption industries include information, financial services, and professional and business services, whereas high-exposure, low-adoption industries include manufacturing and utilities. By contrast, among low-adoption industries, mid- and high-exposure groups exhibit little difference in reallocation activity.

Table A.1: INDUSTRY CLASSIFICATION BY AI EXPOSURE AND ADOPTION

Group	Industries
Low Exposure / Low Adoption	Construction; Transportation and Warehousing; Leisure and Hospitality; Other Services
Low / High	Natural Resources and Mining
Mid / Low	Retail Trade; Education and Health Services
Mid / High	Manufacturing; Utilities
High / Low	Wholesale Trade
High / High	Information; Financial Activities; Professional and Business Services

Notes: Industries are classified each quarter based on terciles of AI exposure (OpenAI measure) and a median split of AI adoption (Lightcast).

A.2 Cross-sectional decomposition

[Decomposition of aggregate unemployment with heterogeneous transition rates] Let aggregate unemployment be

$$u_t = \sum_i \omega_{i,t} u_{i,t}, \qquad u_{i,t} = \frac{s_{i,t}}{s_{i,t} + f_{i,t}}, \tag{A.1}$$

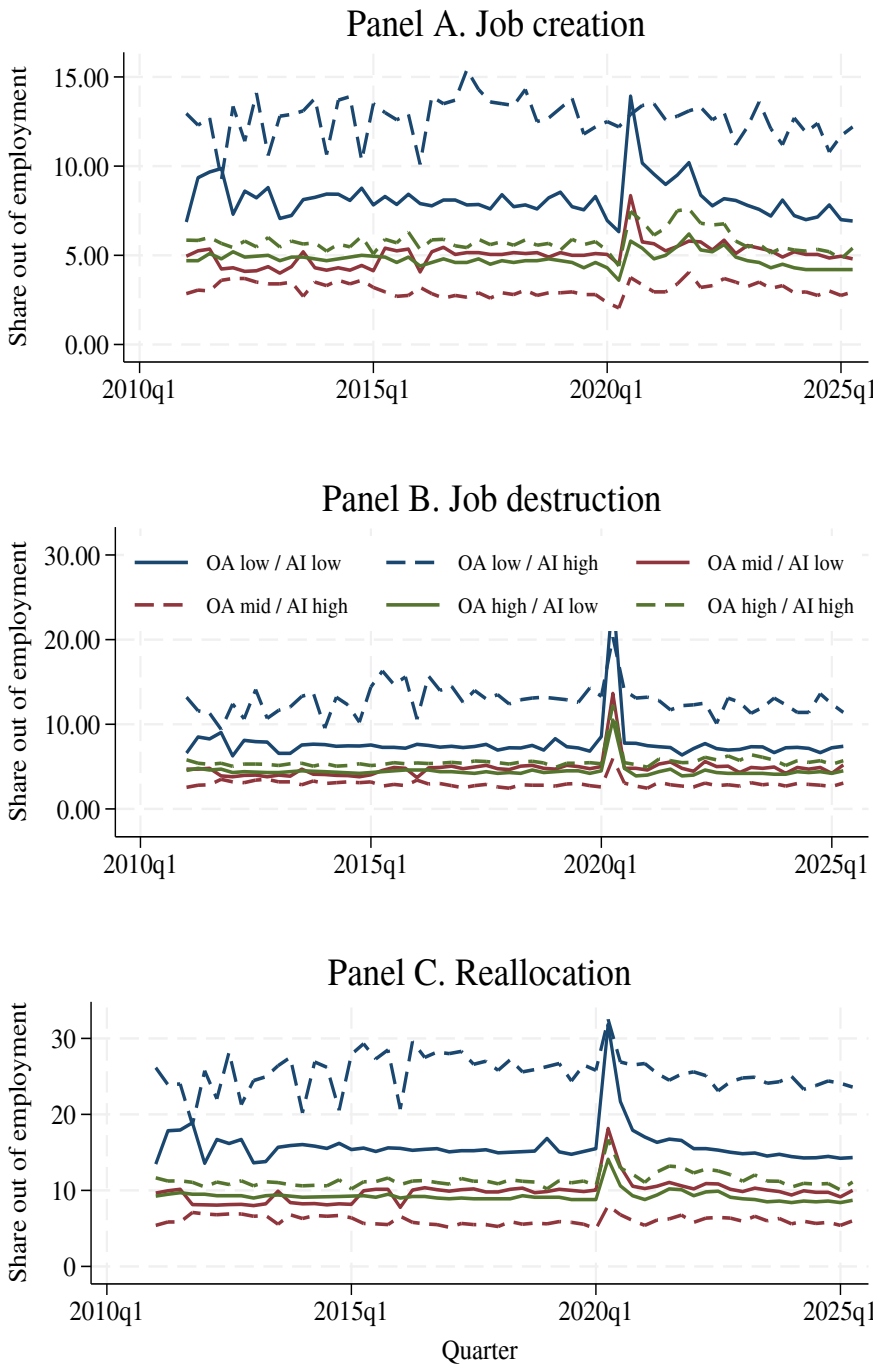
where $\omega_{i,t}$ denotes the labor-force share of group i, $s_{i,t}$ its separation rate, and $f_{i,t}$ its job-finding rate. Define

$$\bar{s}_t = \sum_i \omega_{i,t} s_{i,t}, \qquad \bar{f}_t = \sum_i \omega_{i,t} f_{i,t}, \tag{A.2}$$

and the cross-sectional second moments

$$\mathsf{Var}_t(s_i) = \sum_i \omega_{i,t} (s_{i,t} - \bar{s}_t)^2, \tag{A.3}$$

Figure A.1: JOB FLOWS BY AI EXPOSURE AND ADOPTION



Note: This figure plots the fractions of job creation and job destruction relative to payroll employment by AI exposure and adoption in Panels A and B, respectively. Panel C displays the total reallocation rate, defined as the sum of job creation and destruction, by AI exposure and adoption.

Source: Authors' calculation.

$$\mathsf{Var}_t(f_i) = \sum_i \omega_{i,t}(f_{i,t} - \bar{f}_t)^2, \tag{A.4}$$

$$\mathsf{Cov}_t(s_i, f_i) = \sum_i \omega_{i,t}(s_{i,t} - \bar{s}_t)(f_{i,t} - \bar{f}_t). \tag{A.5}$$

Then, up to a second-order approximation,

$$\Delta u_t \approx \underbrace{\Delta\left(\frac{\bar{s}_t}{\bar{s}_t + \bar{f}_t}\right)}_{\text{mean transition-rate effect}} + \underbrace{\Delta\left(\frac{-\bar{f}_t \mathsf{Var}_t(s_i) + \bar{s}_t \mathsf{Var}_t(f_i) + (\bar{s}_t - \bar{f}_t)\mathsf{Cov}_t(s_i, f_i)}{(\bar{s}_t + \bar{f}_t)^3}\right)}_{\text{dispersion effect}} + \underbrace{\sum_i \Delta\omega_{i,t} \frac{s_{i,t}}{s_{i,t} + f_{i,t}}}_{\text{composition effect}}, \tag{A.6}$$

where $\Delta u_t = u_{t+1} - u_t$ and $\Delta\omega_{i,t} = \omega_{i,t+1} - \omega_{i,t}$.

Proof. Let

$$\phi(s, f) = \frac{s}{s + f}.$$

Then aggregate unemployment can be written as

$$u_t = \sum_i \omega_{i,t}\phi(s_{i,t}, f_{i,t}). \tag{A.7}$$

We derive the result in three steps.

Step 1: Exact within-group and composition decomposition.

By definition,

$$\Delta u_t = \sum_i \omega_{i,t+1}\phi(s_{i,t+1}, f_{i,t+1}) - \sum_i \omega_{i,t}\phi(s_{i,t}, f_{i,t}). \tag{A.8}$$

Add and subtract $\sum_i \omega_{i,t+1}\phi(s_{i,t}, f_{i,t})$ to obtain

$$\Delta u_t = \sum_i \omega_{i,t+1}\Big[\phi(s_{i,t+1}, f_{i,t+1}) - \phi(s_{i,t}, f_{i,t})\Big] + \sum_i \Delta\omega_{i,t}\phi(s_{i,t}, f_{i,t}). \tag{A.9}$$

The second term is the exact composition effect.

Step 2: Second-order approximation of the level of unemployment.

Define deviations from the weighted means:

$$\tilde{s}_{i,t} = s_{i,t} - \bar{s}_t, \qquad \tilde{f}_{i,t} = f_{i,t} - \bar{f}_t.$$

A second-order Taylor expansion of $\phi(s_{i,t}, f_{i,t})$ around $(\bar{s}_t, \bar{f}_t)$ gives

$$\begin{aligned}\phi(s_{i,t}, f_{i,t}) \approx \phi(\bar{s}_t, \bar{f}_t) + \phi_s(\bar{s}_t, \bar{f}_t)\tilde{s}_{i,t} + \phi_f(\bar{s}_t, \bar{f}_t)\tilde{f}_{i,t} \\ + \frac{1}{2}\phi_{ss}(\bar{s}_t, \bar{f}_t)\tilde{s}^2_{i,t} + \phi_{sf}(\bar{s}_t, \bar{f}_t)\tilde{s}_{i,t}\tilde{f}_{i,t} + \frac{1}{2}\phi_{ff}(\bar{s}_t, \bar{f}_t)\tilde{f}^2_{i,t}.\end{aligned} \tag{A.10}$$

The derivatives are

$$\phi_s(s,f) = \frac{f}{(s+f)^2}, \qquad \phi_f(s,f) = -\frac{s}{(s+f)^2}, \tag{A.11}$$

$$\phi_{ss}(s,f) = -\frac{2f}{(s+f)^3}, \qquad \phi_{ff}(s,f) = \frac{2s}{(s+f)^3}, \tag{A.12}$$

$$\phi_{sf}(s,f) = \frac{s-f}{(s+f)^3}. \tag{A.13}$$

Taking weighted averages of (A.10) and using

$$\sum_i \omega_{i,t}\tilde{s}_{i,t} = 0, \qquad \sum_i \omega_{i,t}\tilde{f}_{i,t} = 0,$$

yields

$$u_t \approx \phi(\bar{s}_t, \bar{f}_t) + \frac{1}{2}\phi_{ss}(\bar{s}_t, \bar{f}_t)\mathsf{Var}_t(s_i) + \phi_{sf}(\bar{s}_t, \bar{f}_t)\mathsf{Cov}_t(s_i, f_i) + \frac{1}{2}\phi_{ff}(\bar{s}_t, \bar{f}_t)\mathsf{Var}_t(f_i). \tag{A.14}$$

Substituting the derivatives from (A.13),

$$u_t \approx \frac{\bar{s}_t}{\bar{s}_t + \bar{f}_t} + \frac{-\bar{f}_t\mathsf{Var}_t(s_i) + \bar{s}_t\mathsf{Var}_t(f_i) + (\bar{s}_t - \bar{f}_t)\mathsf{Cov}_t(s_i, f_i)}{(\bar{s}_t + \bar{f}_t)^3}. \tag{A.15}$$

Step 3: Difference over time.

Taking first differences of (A.15) gives

$$\Delta u_t \approx \Delta\left(\frac{\bar{s}_t}{\bar{s}_t+\bar{f}_t}\right)+\Delta\left(\frac{-\bar{f}_t\,\mathsf{Var}_t(s_i)+\bar{s}_t\,\mathsf{Var}_t(f_i)+(\bar{s}_t-\bar{f}_t)\mathsf{Cov}_t(s_i,f_i)}{(\bar{s}_t+\bar{f}_t)^3}\right). \tag{A.16}$$

Combining (A.16) with the exact composition term in (A.9) yields

$$\Delta u_t \approx \Delta\left(\frac{\bar{s}_t}{\bar{s}_t+\bar{f}_t}\right)+\Delta\left(\frac{-\bar{f}_t\,\mathsf{Var}_t(s_i)+\bar{s}_t\,\mathsf{Var}_t(f_i)+(\bar{s}_t-\bar{f}_t)\mathsf{Cov}_t(s_i,f_i)}{(\bar{s}_t+\bar{f}_t)^3}\right)+\sum_i \Delta\omega_{i,t}\,\phi(s_{i,t},f_{i,t}), \tag{A.17}$$

which is (A.6). □

Equation (A.6) implies that changes in aggregate unemployment can be decomposed into three components: a *mean transition-rate effect*, a *dispersion effect*, and a *composition effect*. The dispersion term shows that unemployment rises with greater dispersion in job-finding rates, falls with greater dispersion in separation rates, and depends also on the covariance between the two transition rates.

Derivation of the final decomposition. Let aggregate unemployment be

$$u_t=\sum_i \omega_{i,t}u_{i,t}, \qquad u_{i,t}=\frac{s}{s+f_{i,t}}, \tag{A.18}$$

where s is a common separation rate and $f_{i,t}$ is the job-finding rate of group i. Under the approximation $s \ll f_{i,t}$,

$$u_{i,t}\approx\frac{s}{f_{i,t}}, \tag{A.19}$$

so that

$$u_t \approx s\sum_i \omega_{i,t}\frac{1}{f_{i,t}} = s\,\mathbb{E}_t\left[\frac{1}{f_{i,t}}\right]. \tag{A.20}$$

Let

$$\bar{f}_t=\sum_i \omega_{i,t}f_{i,t}, \qquad \sigma^2_{f,t}=\sum_i \omega_{i,t}(f_{i,t}-\bar{f}_t)^2.$$

A second-order Taylor expansion of $1/f_{i,t}$ around $\bar{f}_t$ gives

$$\frac{1}{f_{i,t}} \approx \frac{1}{\bar{f}_t} - \frac{1}{\bar{f}_t^2}(f_{i,t} - \bar{f}_t) + \frac{1}{\bar{f}_t^3}(f_{i,t} - \bar{f}_t)^2. \tag{A.21}$$

Taking weighted averages and using

$$\sum_i \omega_{i,t}(f_{i,t} - \bar{f}_t) = 0,$$

yields

$$\mathbb{E}_t\left[\frac{1}{f_{i,t}}\right] \approx \frac{1}{\bar{f}_t} + \frac{\sigma_{f,t}^2}{\bar{f}_t^3}. \tag{A.22}$$

Hence

$$u_t \approx \frac{s}{\bar{f}_t} + s\frac{\sigma_{f,t}^2}{\bar{f}_t^3}. \tag{A.23}$$

Taking first differences,

$$\Delta u \approx s\,\Delta\left(\frac{1}{\bar{f}_t}\right) + s\,\Delta\left(\frac{\sigma_{f,t}^2}{\bar{f}_t^3}\right). \tag{A.24}$$

To make the composition effect explicit, return to (A.20):

$$u_t \approx s\sum_i \omega_{i,t}\frac{1}{f_{i,t}}. \tag{A.25}$$

Then

$$\Delta u \approx s\sum_i \omega_{i,t+1}\frac{1}{f_{i,t+1}} - s\sum_i \omega_{i,t}\frac{1}{f_{i,t}} \tag{A.26}$$

$$= s\sum_i \omega_{i,t+1}\left(\frac{1}{f_{i,t+1}} - \frac{1}{f_{i,t}}\right) + s\sum_i \Delta\omega_i \frac{1}{f_{i,t}}. \tag{A.27}$$

The first term is the within-group effect and the second term is the composition effect.

Using the second-order approximation for the within-group term implies

$$s\sum_i \omega_{i,t+1}\left(\frac{1}{f_{i,t+1}}-\frac{1}{f_{i,t}}\right)\approx s\Delta\left(\frac{1}{\bar{f}_t}\right)+s\Delta\left(\frac{\sigma^2_{f,t}}{\bar{f}^3_t}\right). \tag{A.28}$$

Therefore, the final decomposition is

$$\Delta u \approx \underbrace{s\Delta\left(\frac{1}{\bar{f}_t}\right)}_{\text{mean job-finding change}} + \underbrace{s\Delta\left(\frac{\sigma^2_{f,t}}{\bar{f}^3_t}\right)}_{\text{dispersion in } f_i} + \underbrace{s\sum_i \Delta\omega_i \frac{1}{f_{i,t}}}_{\text{composition shifts}}. \tag{A.29}$$

Job-finding rate and AI exposure. Let U_{kt} denote an indicator equal to one if individual k is unemployed at time t, and let $UE_{k,t+1}$ denote an indicator equal to one if the individual transitions from unemployment at time t to employment at time $t+1$. Let $a_{kt} \in [0,1]$ denote the individual's AI exposure, and let w_{kt} be the sampling weight.

We define the job-finding rate at AI exposure a as

$$m_t(a) \equiv P(E_{k,t+1}=1 \mid U_{kt}=1,\ a_{kt}=a) = \frac{E\left[w_{kt}UE_{k,t+1} \mid a_{kt}=a\right]}{E[w_{kt}U_{kt} \mid a_{kt}=a]}. \tag{A.30}$$

The aggregate job-finding rate is given by

$$\bar{m}_t = P(E_{k,t+1}=1 \mid U_{kt}=1) = \frac{\sum_k w_{kt}UE_{k,t+1}}{\sum_k w_{kt}U_{kt}} = \int_0^1 m_t(a)\, dF^U_t(a), \tag{A.31}$$

where $F^U_t(a)$ denotes the cross-sectional distribution of AI exposure among unemployed workers at time t.

Variance decomposition. Let $Y^{UE}_{k,t+1} \equiv \mathbf{1}\{E_{k,t+1}=1\}$ for individuals with $U_{kt}=1$. Then

$$m_t(a) = E\left[Y^{UE}_{k,t+1} \mid U_{kt}=1,\ a_{kt}=a\right]. \tag{A.32}$$

The cross-sectional variance of job-finding outcomes among the unemployed admits the

decomposition

$$\mathrm{Var}_t\Big(Y^{UE}_{k,t+1} \mid U_{kt}=1\Big) = \underbrace{\mathrm{Var}_t\big(m_t(a_{kt}) \mid U_{kt}=1\big)}_{\text{between-AI component}} + \underbrace{E_t\Big[\mathrm{Var}_t\Big(Y^{UE}_{k,t+1} \mid U_{kt}=1,\ a_{kt}\Big)\Big|U_{kt}=1\Big]}_{\text{within-AI component}}. \quad \text{(A.33)}$$

Since $Y^{UE}_{k,t+1}$ is binary, we have

$$\mathrm{Var}_t\Big(Y^{UE}_{k,t+1} \mid U_{kt}=1,\ a_{kt}=a\Big) = m_t(a)\big(1-m_t(a)\big). \quad \text{(A.34)}$$

Therefore,

$$\mathrm{Var}_t\Big(Y^{UE}_{k,t+1} \mid U_{kt}=1\Big) = \int_0^1 \big(m_t(a)-\bar{m}_t\big)^2\, dF^U_t(a) + \int_0^1 m_t(a)\big(1-m_t(a)\big)\, dF^U_t(a). \quad \text{(A.35)}$$

Variance attributable to AI exposure. The component of cross-sectional variation in job-finding rates attributable to AI exposure is given by

$$\mathrm{Var}^{AI}_t = \mathrm{Var}_t\big(m_t(a_{kt}) \mid U_{kt}=1\big) = \int_0^1 \big(m_t(a)-\bar{m}_t\big)^2\, dF^U_t(a). \quad \text{(A.36)}$$

Sample analog. Define normalized weights over the unemployed as

$$\tilde{w}^U_{kt} = \frac{w_{kt}U_{kt}}{\sum_\ell w_{\ell t}U_{\ell t}}. \quad \text{(A.37)}$$

Then the sample analogs are

$$\bar{m}_t = \sum_k \tilde{w}^U_{kt}\, UE_{k,t+1}, \quad \text{(A.38)}$$

and

$$\widehat{\mathrm{Var}}^{AI}_t = \sum_k \tilde{w}^U_{kt}\big(\hat{m}_t(a_{kt})-\bar{m}_t\big)^2, \quad \text{(A.39)}$$

where $\hat{m}_t(a)$ is an estimate of $m_t(a)$ obtained, for example, via binning or nonparametric smoothing.

B Additional decomposition results

Figure A.2 displays the dispersion in job-finding rates (solid blue line) attributable to AI (red dashed line) and to residual factors (green dotted line) in the upper panel, along with their respective shares of total dispersion in the lower panel.

C Additional regression results

Table A.2 reports the regression results for usual hours worked.

Figure A.2: WITHIN-INDUSTRY DISPERSION OF JOB-FINDING RATES

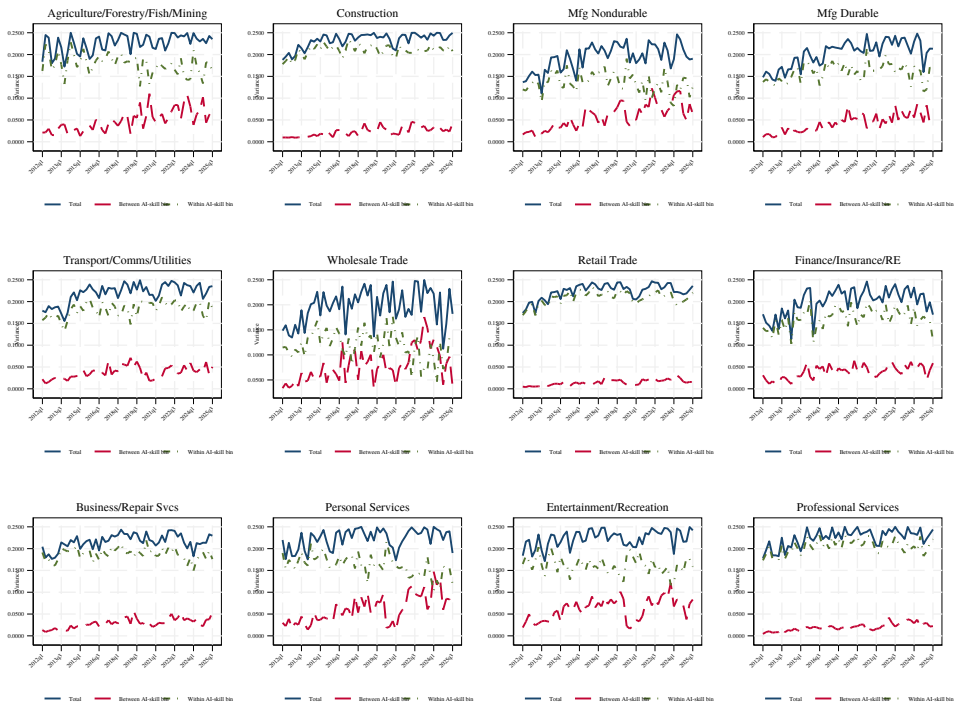


Table A.2: DETERMINANTS OF USUAUL HOURS

	(1) WO industry FE	(2) W/ industry FE
AI exposure	3.707***	3.252***
	(0.0668)	(0.0726)
AI exposure × LLM period	-0.471***	-0.449***
	(0.154)	(0.151)
AI skill share	-6.932***	-7.567***
	(0.788)	(0.801)
AI skill share × LLM period	3.999***	4.684***
	(1.098)	(1.097)
Market tightness	0.00615***	0.00510***
	(0.000550)	(0.000549)
Age	1.129***	1.031***
	(0.00617)	(0.00614)
Age squared	-0.0123***	-0.0112***
	(0.0000690)	(0.0000684)
Female	-4.409***	-3.579***
	(0.0239)	(0.0267)
High-school graduation	2.288***	2.086***
	(0.0557)	(0.0550)
Some college and associate degree	2.017***	1.952***
	(0.0568)	(0.0567)
College graduation	3.272***	3.423***
	(0.0567)	(0.0579)
Observations	756421	756420
R-squared	0.116	0.143

Standard errors in parentheses

Time fixed effects are included in both columns.

* $p < 0.10$, ** $p < 0.05$, *** $p < 0.01$

D Estimation of Bayesian trend-cycle decomposition

Bayesian estimation. We estimate the model in a Bayesian state-space framework. Let y_t denote the vector of observables at time t, which in our setting consists of the unemployment inflow and outflow rates for each group $g \in \{H, L\}$. The model can be written in state-space form with a measurement equation linking the observed series to latent trend and cyclical components, and a transition equation governing the evolution of the latent states over time.

Specifically, let the state vector collect the latent components,

$$\alpha_t = \begin{bmatrix} \tau^s_{Ht} & \tau^s_{Lt} & \tau^f_{Ht} & \tau^f_{Lt} & \beta^f_{Ht} & \beta^f_{Lt} & c^s_{Ht} & c^s_{Lt} & c^f_{Ht} & c^f_{Lt} \end{bmatrix}'.$$

The measurement equation is

$$y_t = Z\alpha_t + \varepsilon_t, \qquad \varepsilon_t \sim \mathcal{N}(0, H), \tag{D.1}$$

where Z is the selection matrix mapping latent states into the observed inflow and outflow rates, and H is the covariance matrix of measurement errors. In the benchmark specification, the observed group-specific inflow and outflow rates are the sum of their corresponding trend and cyclical components.

The transition equation is

$$\alpha_t = T\alpha_{t-1} + R\xi_t, \qquad \xi_t \sim \mathcal{N}(0, Q), \tag{D.2}$$

where T encodes the law of motion of the latent states, R is a selection matrix, and Q is the covariance matrix of state innovations. In our application, the trend in the inflow rate is specified as a local level, while the trend in the outflow rate is specified as a local linear trend. The cyclical components may be modeled as stationary autoregressive processes. More concretely, a

stochastic version of the model is given by

$$\tau^s_{gt} = \tau^s_{g,t-1} + \nu^s_{gt}, \tag{D.3}$$

$$\tau^f_{gt} = \tau^f_{g,t-1} + \beta^f_{g,t-1} + \nu^f_{gt}, \tag{D.4}$$

$$\beta^f_{gt} = \beta^f_{g,t-1} + \kappa^f_{gt}, \tag{D.5}$$

$$c^s_{gt} = \phi^s_g c^s_{g,t-1} + \omega^s_{gt}, \tag{D.6}$$

$$c^f_{gt} = \phi^f_g c^f_{g,t-1} + \omega^f_{gt}, \tag{D.7}$$

with Gaussian shocks

$$\nu^s_{gt} \sim \mathcal{N}(0, \sigma^2_{\nu^s,g}), \quad \nu^f_{gt} \sim \mathcal{N}(0, \sigma^2_{\nu^f,g}), \quad \kappa^f_{gt} \sim \mathcal{N}(0, \sigma^2_{\kappa^f,g}),$$

and similarly for the cyclical shocks. Even if the exposition in the main text suppresses the innovation terms for simplicity, Bayesian estimation is naturally implemented using the stochastic state-space representation above.

Likelihood and posterior distribution. Conditional on the parameter vector Θ, the likelihood function can be evaluated using the Kalman filter. Let

$$\Theta = \{H, Q, \phi^s_g, \phi^f_g, \text{initial states and their variances}\}.$$

Given Θ, the Kalman filter recursively produces the one-step-ahead prediction errors and their covariance matrices, which together imply the Gaussian likelihood,

$$p(y_{1:T} \mid \Theta) = \prod_{t=1}^{T} p(y_t \mid y_{1:t-1}, \Theta). \tag{D.8}$$

Bayesian inference combines this likelihood with prior distributions on the parameters:

$$p(\Theta \mid y_{1:T}) \propto p(y_{1:T} \mid \Theta)\, p(\Theta). \tag{D.9}$$

The posterior distribution of the latent states is obtained jointly with the posterior of the structural parameters.

Prior distributions. We use priors that enforce economically and statistically sensible restrictions while remaining weakly informative. Variance parameters are restricted to be positive, so they are assigned inverse-gamma, half-normal, or half-Cauchy priors. For example,

$$\sigma_{\nu^s,g}, \sigma_{\nu^f,g}, \sigma_{\kappa^f,g} \sim \mathcal{N}^+(0, \bar{\sigma}^2),$$

where $\mathcal{N}^+$ denotes the half-normal distribution. Autoregressive coefficients governing the cycles are restricted to the stationary region,

$$\phi_g^s, \phi_g^f \in (-1, 1),$$

and may be assigned transformed beta priors centered on moderate persistence. Initial states are assigned diffuse Gaussian priors,

$$\alpha_0 \sim \mathcal{N}(a_0, P_0),$$

with P_0 chosen sufficiently large to reflect prior uncertainty.

The priors can also be used to regularize the relative smoothness of the trends. In particular, the variances of the trend innovations determine the extent to which the latent trends are allowed to move over time. Small values of $\sigma^2_{\nu^s,g}$ imply a smoother trend in inflow rates, while larger values permit more time variation. Similarly, $\sigma^2_{\kappa^f,g}$ controls the smoothness of the slope in job-finding trends. This feature is especially useful in relatively short samples or when the data

are noisy, because it prevents the estimated trends from absorbing high-frequency fluctuations that are better interpreted as cyclical.

Posterior simulation. Because the posterior distribution is not available in closed form, we simulate from it using Markov chain Monte Carlo (MCMC). A convenient strategy is a Gibbs sampler with Metropolis-Hastings steps for parameters whose conditional posterior distributions are not of standard form.

A typical sampling algorithm proceeds as follows:

1. Initialize the parameter vector $\Theta^{(0)}$.
2. Conditional on $\Theta^{(m-1)}$, draw the full path of latent states $\alpha_{1:T}^{(m)}$ using the Carter–Kohn simulation smoother or the Durbin–Koopman simulation smoother.
3. Conditional on $\alpha_{1:T}^{(m)}$, draw variance parameters from their conditional posterior distributions.
4. Conditional on $\alpha_{1:T}^{(m)}$, draw autoregressive coefficients and any remaining hyperparameters, using direct draws where possible and Metropolis-Hastings updates otherwise.
5. Repeat steps 2–4 for $m = 1, \ldots, M$, discard burn-in draws, and retain the remaining draws for posterior inference.

The key advantage of this approach is that it integrates over uncertainty in both the latent states and the model parameters. Rather than treating the trend components as fixed objects estimated in a preliminary step, Bayesian estimation jointly infers trends, cycles, and hyperparameters in one coherent framework.

Recovery of the natural rate. For each posterior draw m, we recover the group-specific natural rate as

$$u_{gt}^{*,(m)} = \frac{\tau_{gt}^{s,(m)}}{\tau_{gt}^{s,(m)} + \tau_{gt}^{f,(m)}}, \tag{D.10}$$

and aggregate across groups using labor force shares:

$$u_t^{*,(m)} = \sum_{g \in \{H,L\}} \omega_{gt}\, u_{gt}^{*,(m)}. \tag{D.11}$$

Posterior means, medians, and credible intervals for u_{gt}^* and u_t^* are then constructed directly from the retained MCMC draws. This procedure transparently propagates uncertainty in latent inflow and outflow trends into uncertainty about the natural rate itself.

Advantages of the Bayesian approach. The Bayesian framework offers several advantages in this setting. First, it is well suited to latent-variable models in which the objects of interest—trend inflow rates, trend outflow rates, and group-specific natural rates—are not directly observed. Second, it provides a coherent way to impose economically sensible restrictions, such as smoothness of trends and stationarity of cycles, through the prior. Third, posterior credible intervals reflect multiple sources of uncertainty simultaneously: uncertainty about latent states, uncertainty about hyperparameters, and uncertainty about measurement noise. This is particularly important when the sample is not long, when one subgroup is relatively small, or when the decomposition between trend and cycle is empirically delicate.

A further advantage is that the Bayesian framework makes nonlinear transformations straightforward. The natural rate is a nonlinear function of the latent trend components, but posterior simulation immediately delivers its full distribution at each date. In contrast, frequentist inference for such nonlinear functions often requires additional approximations, such as the delta method or bootstrap procedures.

Practical implementation. In practice, estimation proceeds separately for the model parameters and latent states but jointly within the MCMC algorithm. After checking convergence diagnostics, such as trace plots, effective sample sizes, and potential scale reduction factors, we summarize the posterior distribution using posterior medians and equal-tailed or highest-posterior-density credible intervals. To assess robustness, one can examine alternative prior

choices for trend-innovation variances, different specifications of the cyclical component, and alternative definitions of AI exposure groups.

In addition, because the aggregate natural rate is a weighted average of group-specific natural rates, time variation in labor force shares ω_{gt} can contribute to movements in the aggregate natural rate even when group-specific trends are unchanged. The Bayesian framework accommodates this naturally by recomputing the aggregate object at each posterior draw and date.

Interpretation. The resulting estimates allow us to distinguish between changes in unemployment driven by cyclical fluctuations and changes driven by low-frequency shifts in trend inflow and outflow rates. In particular, the model quantifies whether the natural rate for AI-exposed workers has risen or fallen relative to that for AI-nonexposed workers, and whether any change in the aggregate natural rate reflects changes in within-group trend labor market dynamics or changes in the composition of the labor force across exposure groups.